Energy & Environmental Science

REVIEW

View Article Online
View Journal | View Issue

CrossMark click for updates

Cite this: *Energy Environ. Sci.*, 2015, **8**, 1110

Olivine $LiFePO_4$: the remaining challenges for future energy storage

Jiajun Wang† and Xueliang Sun*

Received 20th December 2014
Accepted 22nd January 2015

DOI: 10.1039/c4ee04016c

www.rsc.org/ees

Rechargeable batteries can effectively store electrical energy as chemical energy, and release it when needed, providing a good choice for applications in electric vehicles (EVs). Naturally, safety concerns are the key issue for the application of battery technology in EVs. Olivine $LiFePO_4$ is considered to be the most promising cathode material for lithium-ion batteries due to its environmental friendliness, high cycling performance and safety characteristics. Some important breakthroughs in recent years have allowed its successful commercialization. However, in spite of its success, the commercial application of $LiFePO_4$ batteries in EVs is still hindered by some technological obstacles. Herein, we provide an update on our previous review, and overview the most significant advances in the remaining challenges for this promising battery material. New research directions and future trends have also been discussed.

Broader context

Since the first report in 1997, olivine $LiFePO_4$ has been considered as the most competitive cathode material for electric vehicles due to its high thermal stability and safety; therefore, numerous efforts have been made to understand and improve the performance of $LiFePO_4$. In spite of some breakthrough advances, the large-scale application of $LiFePO_4$ batteries in transportation still encounters many technical obstacles. In our previous review paper, we mainly discussed carbon coating technology, one of the most important breakthroughs in $LiFePO_4$ development. In combination with the latest advances in $LiFePO_4$ field, herein we provide an updated overview of current research activities and highlight some key challenges (fast-charging, lithiation–delithiation mechanism, and surface chemistry stability) for future $LiFePO_4$ development. These obstacles necessitate a better understanding of $LiFePO_4$ under *in situ* or *in operando* conditions; as a result, the application of advanced synchrotron X-ray technology (mainly imaging tools) is also briefly summarized. In addition, considering the new research trend in next-generation battery systems, an up-to-date understanding and exploration of olivine phosphate for Na-ion batteries could also be expected to open up new research hotspots in energy storage field. A couple of practical issues with strong industrial interests are also included.

1. Introduction

Since the first report in 1997 by Goodenough *et al.*[1] lithium iron phosphate has become one of the hottest cathode materials in the field of battery research. In particular, in recent years the considerable demands for a high safety and high-performance large-scale energy storage system in electric vehicles has inspired numerous research studies to optimize this cathode material, which have been summarized in several excellent review papers.[2–5] With size reduction to the nanoscale and carbon coating strategies,[6–8] the formerly poor intrinsic electronic and ionic conductivity have been enormously improved and commercial $LiFePO_4$ batteries have now begun to be used in electric vehicles. Despite the superior thermal safety, high reversibility and acceptable operating voltage (3.45 *vs.* Li^+/Li) making $LiFePO_4$ more competitive than other cathode materials; there is still a long way to go before $LiFePO_4$ can be used for large-scale application in electric vehicles and many technical challenges remain unsolved.

One challenge is related to the demands for fast-charging in EV's batteries.[9] Compared to the electronic conductivity, ionic conductivity or lithium-ion diffusion plays a dominate role in determining the electrochemical reaction kinetics. It is widely accepted that the electrochemical delithiation reaction proceeds *via* a two-phase process between the two end members of $LiFePO_4$ and $FePO_4$,[10] and that lithium ions diffuse along a 1-dimensional pathway with a preferential (010) direction,[11] hindering the fast lithium ion insertion/extraction. Although the rate performance of $LiFePO_4$ has been improved by shortening the diffusion distance with the size reduction,[12,13] it is still not able to satisfy the high rate expectations of EVs. Despite the success of some conventional engineering methods, a breakthrough in high rate performance is still needed, which heavily relies on a fundamental understanding of the lithium diffusion kinetics and the underlying phase transformation mechanism. The exploration and development of a number of *in situ* experimental techniques,[14–18] particularly in recent years, poses new opportunities to shed light on previous controversial models and to suggest possible solutions to the high rate

Department of Mechanical and Materials Engineering, University of Western Ontario, London, Ontario, N6A 5B9, Canada. E-mail: xsun@eng.uwo.ca; Tel: +1 5196612111 ext. 87759

† Present address: National Synchrotron Light Source II, Brookhaven National Laboratory, Upton, NY, 11973, USA.

performance issue. An obvious trend is that of a single-phase mechanism or solid solution model confirmed by different experiments,[19–22] which enrich previous mechanism elucidation and also provide new theoretical guidelines for further high rate $LiFePO_4$ battery materials.

The other challenge is the surface chemistry stability in $LiFePO_4$. In general, due to the strong P–O covalent bonds in the olivine structure prohibiting oxygen release, $LiFePO_4$ is considered to have a superior thermal stability. Nevertheless, actual $LiFePO_4$ batteries are not always as stable as expected; for instance, performance degradation always occurs with electrochemical cycling,[23,24] which is considered to be due to moisture contamination. Many research interests have targeted understanding the surface chemistry change or aging process when moisture contamination is present, including in storage and in the electrochemical working conditions.[24–26] In addition, considering the strong reducing environment and high temperatures during the carbon-coating process, the possible surface chemistry change of $LiFePO_4$ has attracted much attention, as the $LiFePO_4$ surface and the interface between carbon and $LiFePO_4$ directly affect the electronic and ion conductivity.

Another research trend is the development of a novel olivine family for next-generation battery systems. Because of their low cost and wide availability, sodium ion batteries have recently been pursued as potential alternatives to current lithium-ion batteries.[27,28] Encouraged by the tremendous success of olivine $LiFePO_4$ in lithium-ion batteries, the analogous $NaFePO_4$ was expected to show similar properties as $LiFePO_4$; however, this is not always the case. Recent studies have shown a significant difference between $NaFePO_4$ and $LiFePO_4$, including their electrochemical properties (capacity, reversibility, cycle performance), phase transformation mechanism and synthesis routes.[29,30]

In our previous review,[31] we focused on the progress and development of carbon-coating methods for $LiFePO_4$. Considering this popular battery material and its recent important progress, herein, we present an updated review, mainly based on the latest two year's literature and extend our discussion to focus on new aspects of the aforementioned actively studied topics in olivine $LiFePO_4$, including performance optimizing strategies, understanding of the insertion/extraction mechanism *via in situ* methods, surface chemistry stability and the future use of olivine phosphate for sodium-ion batteries. Some perspectives and suggestions with regard to future research directions and challenges are also provided.

2. Strategies for performance improvement

2.1. Optimizing the carbon coating

Carbon coating on $LiFePO_4$ is a widely accepted method to improve the battery material's conductivity. Generally, the carbon-coating process involves mixing battery materials with various carbon precursors followed by high-temperature thermal treatment. This approach is simple, feasible and suitable for large-scale industrial production. However, the control of a uniform coating layer and improving the carbon quality is still very challenging. Too thin of a carbon coating layer will not cover the active material uniformly, but too thick of a carbon coating will limit lithium ion diffusion and decrease the volumetric energy density of the battery materials. To meet the demands for high performance battery materials, current carbon-coating technology still needs to be further improved. This can be done in a number of ways.

First, to optimize the carbon-coating quality for $LiFePO_4$, the selection of a high quality carbon source is critical.[32,33] A variety

Dr Jiajun Wang earned his PhD in electrochemistry at Harbin Institute of Technology, China. His PhD thesis focused on the durability study of electrode materials in proton exchange membrane fuel cells. After his PhD studies, he joined Prof. Sun's group at the University of Western Ontario, where he was engaged in an industrial project sponsored by Phostech Lithium Inc. to understand the surface and interface behavior in carbon-coated $LiFePO_4$. Meanwhile, he also partially worked in the field of lithium–air batteries research. Dr Wang has broad research experience in electrochemistry, nanomaterial fabrication/characterization, synchrotron techniques and in clean energy fields. Currently, he is working at the National Synchrotron Light Source II, Brookhaven National Laboratory, to develop an in situ and in operando synchrotron X-ray method for energy materials research.

Professor Xueliang (Andy) Sun is a Senior Canada Research Chair (Tier 1) and Full Professor at the University of Western Ontario, Canada. Dr Sun received his PhD in Materials Chemistry under the direction of Prof. George Thompson in 1999 at the University of Manchester, UK, which he followed up by working as a postdoctoral fellow under the direction of Prof. Keith Mitchell at the University of British Columbia, Canada and as a Research Associate under the direction of Prof. Jean-Pol Dodelet at l'Institut national de la recherche scientifique (INRS), Canada. His current research interests are associated with advanced materials for electrochemical energy storage and conversion, including electrocatalysis and catalyst support in fuel cells and electrodes in lithium-ion batteries and metal–air batteries.

of carbon sources with different chemical and physical properties have been applied to the carbon-coating process for $LiFePO_4$. Some classic carbon sources include some organic sources (*e.g.* glucose, citric acid and lactose) and some inorganic sources (*e.g.* acetylene black, carbon nanotubes and graphene). Organic carbon sources are advantageous in forming a homogeneous carbon-coating layer and in having a good control of the carbon-layer structure (thickness, homogeneity, full coverage) during the pyrolysis process at high temperatures, but the carbon quality (conductivity, graphitized degree) is hard to control. Inorganic carbon provides the opposite advantages and disadvantages. With the selection of high quality inorganic carbon, such as carbon nanotubes and graphene, the entire $LiFePO_4$ electrode can be composed of a 3D conductive network, but local conductive paths in individual $LiFePO_4$ particles (particle surface) may still need to be provided with small amounts of an organic carbon coating. The combination of the advantages of both organic and inorganic carbon sources is more promising for high performance C/$LiFePO_4$ composites.[34]

Second, to maximize the electronic conductivity improvement, a uniform carbon nanolayer with full coverage on $LiFePO_4$ should be first achieved, which is a challenge for many carbon-coating methods. Some *in situ* carbon-coating methods, such as the self-polymerization of dopamine or resorcinol–formaldehyde gel, can result in a uniform carbon-coating layer on $LiFePO_4$; however, a more economic and feasible method is still highly desirable.[35,36] Recently, a novel carbon-coating method *via* the physical evaporation and deposition of carbon under vacuum has been reported.[37] By continuous agitation of the sample, coupled to rotation and tilting of the sample holder, a homogeneous and uniform carbon-coating layer can be obtained. The carbon-coating thickness can be controlled with the deposition time and the physical properties (the conductivity and graphitization degree) of the carbon coating have been proven to be similar to those of the traditional high-temperature treatment method. Despite this, additional improvement is still needed for further large-scale production; however, this method does provide a new route to achieve a high-quality carbon coating on $LiFePO_4$ battery materials.

Third, further modification of the carbon-coating layer *via* nitrogen doping or co-coating (hybrid coating) provides feasible strategies to optimize the carbon coating for $LiFePO_4$. A nitrogen-doped carbon layer has proven to improve the electrical contact/conductivity and prevent $LiFePO_4$ aggregation, thus treated $LiFePO_4$ has been shown to exhibit a superior rate capability and capacity retention.[38] Because of the hydrophilic properties of nitrogen doping, our previous work also indicated that nitrogen-doped carbon nanotubes allow a more uniform dispersion of carbon nanomaterials and thus enhance the electronic contact of $LiFePO_4$.[39] Furthermore, the nitrogen atoms also may contribute additional electrons, providing electron carriers for the conduction band, further improving the electronic conductivity of $LiFePO_4$. In addition to the electronic conductivity improvement, nitrogen also may induce defects to lower the activation energy of lithium ion diffusion, enhancing the lithium ion diffusion kinetics. Therefore, an improved rate performance can be expected by nitrogen-doped carbon coating. The other modification strategy for carbon coating is co-coating carbon with metal oxides or ionic conductors. Metal oxide co-coating may improve the charge transfer resistance, and more importantly, it can improve the surface chemical stability of $LiFePO_4$ by consuming HF created by moisture contamination.[40–42] Ionic conductor (Li_3PO_4 and $CePO_4$ *et al.*) co-coating allows faster lithium ion diffusion. Combined with a highly electronic conductivity carbon coating, this hybrid coating improves the rate performance and low temperature performance of $LiFePO_4$.[43,44] However, the optimized ratio of the ionic/electronic conductor and the controlled hybrid coating method are still challenges for practical $LiFePO_4$ production.

Fourth, in addition to optimizing the carbon-coating layer, another strategy to improve $LiFePO_4$ performance is by the fabrication of additional carbon structures to make up for the deficiencies of the inhomogeneous carbon coating layer. By creating interconnected open pores for electrolyte penetration and by limiting $LiFePO_4$ agglomeration, 3D carbon structures enable faster inter-particle lithium-ion and electron transfer, leading to a high utilization of $LiFePO_4$ particles and a good columbic efficiency.[45,46] For example, Ni *et al.* recently introduced carbon-coated $LiFePO_4$ to a porous carbon structure and fabricated 3D carbon-coated $LiFePO_4$–porous carbon composites. $FePO_4 \cdot 2H_2O$ precursor was first deposited into the porous carbon matrix, and followed by an *in situ* transformation into carbon-coated $LiFePO_4$ with $CH_3COOLi \cdot 2H_2O$ and sucrose as the lithium and carbon sources, respectively. As a result, carbon-coated $LiFePO_4$ particles were well dispersed into the porous carbon matrix. The double carbon structure (carbon nanolayer on the $LiFePO_4$ particles and the additional carbon matrix) created a 3D conductive network, providing fast ionic and electronic conduction, and contributing to the high rate performance of $LiFePO_4$.[47]

Finally, a porous carbon-coating layer is highly expected to improve the performance of $LiFePO_4$. In recent years, the advances in $LiFePO_4$ electric vehicle batteries have placed a higher demand on carbon coatings. In general, the main functions of the carbon coating for $LiFePO_4$ are to improve the electronic conductivity and control the particle size growth at high temperatures. Additionally, for the practical use of $LiFePO_4$ for EVs, carbon coating is also expected to enhance the ionic conductivity in order to achieve a high rate performance. Therefore, a recent research trend in carbon coating has been to develop a porous carbon structure on $LiFePO_4$ which enables the storage of sufficient electrolytes to maximize the electrode reaction interface, and most importantly, to provide a fast lithium-ion transfer pathway.[48,49] Texturally structured carbon aerogels with a large amount of micropores (nanometers) and mesopores (tens of nanometers) are ideal carbon sources, and have attracted much attention recently.[50] With optimizing of the experimental parameters, tuning the pore size and controlling the pore distribution, these porous carbon sources can be expected to play an increasing role in the structural design of future high-rate $LiFePO_4$ materials.

2.2. Advanced carbon composite

In addition to conventional carbon coating *via* the pyrolysis of organic carbon sources, in recent years, the introduction and synthesis of advanced carbon materials, such as graphene and carbon nanotubes, has been widely applied to the improvement of $LiFePO_4$ conductivity, due to their unique character and superior electronic conductivity.

Graphene. Graphene, a monolayer of sp2-bonded carbon atoms or one monolayer of graphite has attracted considerable attention as an advanced carbon additive. The structural flexibility, large specific surface area, high mechanical strength and superior electric conductivity of graphene can build a highly effective 3D conductive network for $LiFePO_4$, which increase the inter-particle electric contact and improve the electrochemical performance of $LiFePO_4$.[51,52] Based on these unique advantages, numerous studies on graphene-modified $LiFePO_4$ have been reported in recent years,[53–56] and graphene/$LiFePO_4$ composites indeed have shown an improved electrochemical performance. Currently, it is generally accepted that the enhanced electrochemical performance of graphene/$LiFePO_4$ is attributed to the inherent features of graphene (excellent electronic conductivity, high surface area, *etc.*). In addition, the introduction of 2D graphene can lead to more uniform $LiFePO_4$ particle dispersion than conventional carbon additives, such as acetylene black, resulting in high electrochemical performance.[57] Furthermore, graphene may lead to an additional capacity for the cathode. A recent report shows that graphene-modified $LiFePO_4$ can charge beyond its theoretical capacity. Hu *et al.* applied 2 wt% graphene to wrap commercial carbon-coated $LiFePO_4$, resulting in a capacity of 208 mA h g^{-1} (the theoretical value is 170 mA h g^{-1} for $LiFePO_4$), as shown in Fig. 1. The authors attributed the extra capacity to the reversible redox reaction between the lithium ions in the electrolyte and exfoliated graphene flakes. If this is the case, this unique feature is also likely applicable to other battery materials.[58]

In spite of these unique features of graphene, the practical application of graphene faces too many challenges. The first challenge is the easy aggregation and poor dispersion of 2D graphene sheets in common solvents, due to its hydrophobic nature, which significantly decreases its advantages.[59,60] Our group studied the impact of stacked and unfolded graphene on $LiFePO_4$ performance. It was found that, compared with stacked graphene with a wrinkled structure (synthesized by the thermal reduction of graphene oxide), unfolded graphene (synthesized by the hydrazine reduction of graphene oxide in solution) enables $LiFePO_4$ to be well dispersed, so that individual $LiFePO_4$ particles are attached to the conductive layer, leading to a higher electronic conductivity and performance, as shown in Fig. 2.[61] To improve graphene dispersion in solution, similar to carbon nanotubes, application of a functionalization treatment with strong oxidizing agents is a common strategy to create hydrophilic carboxyl groups and surface defects.[62–64] However, this violent method also destroys the intact structure of graphene, leading to some loss of its unique mechanical, chemical and physical properties. A mild surface treatment method is highly expected to make full use of its advantages for battery

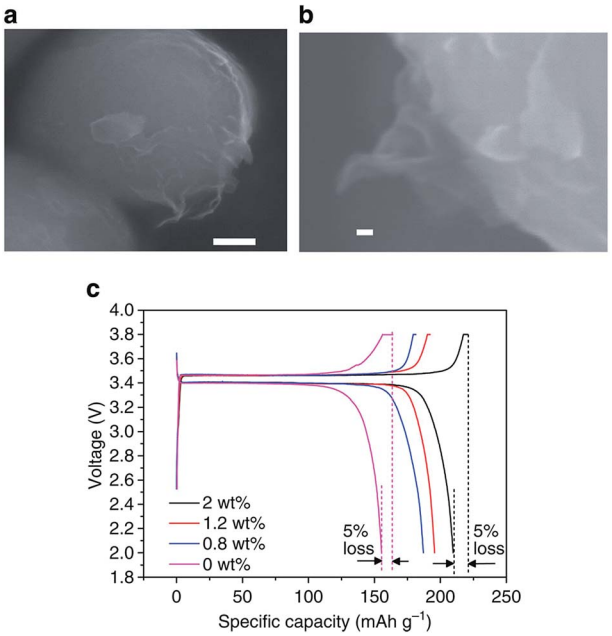

Fig. 1 Morphology and electrochemical performance of a graphene/$LiFePO_4$ composite. (a and b) SEM images of graphene/$LiFePO_4$. Scale bar, 100 nm and 10 nm in (a) and (b), respectively. (c) The first charge/discharge profile at 0.1 C for graphene/$LiFePO_4$ composite with various graphene-loadings (0, 0.8, 1.2 and 2 wt%). Reproduced with permission from ref. 58. Copyright 2014, Nature Publishing Group.

materials.[65,66] Rhodanineacetic acid–pyrene (RAAP) was recently used to functionalize graphene nanosheets due to the strong π–π stacking force between RAAP and thermally exfoliated graphene. As a result, the RAAP molecules were well dispersed on graphene nanosheets and the resulting graphene was negatively charged. Through charge attraction, Fe^{2+} ions and PO_4^{3-} were adsorbed onto RAAP-modified graphene, and subsequently formed $FePO_4$/graphene hybrids. After mixing with $LiCH_3COOH$, the finial $LiFePO_4$/graphene composite was obtained by a thermal reduction process. With this strategy, $LiFePO_4$ particles can be directly grown on graphene with good electronic contact, leading to a high rate capability and capacity retention upon cycling.[67] In addition, nitrogen doping is also a facile method to improve graphene dispersion in solution.

Another challenge for graphene is the development of a simple and facile synthesis method. Most graphene-related $LiFePO_4$ synthesis methods involve complex and time-consuming synthesis processes, such as high temperature post-heating and extensive reflux reactions.[68–70] Although some approaches for mass production of graphene have recently been reported,[71,72] a rapid, economic and feasible approach with a high yield of good crystalline graphene/$LiFePO_4$ material is highly desirable. Microwave-assisted synthesis enables graphene-nanosheet–encapsulated $LiFePO_4$ within a few minutes at low temperatures without any post annealing treatments. This approach makes it possible for the large-scale industrial production of graphene/$LiFePO_4$ composites in the near future.[73] In addition, an ultrasonic-assisted rheological phase method in combination with a carbothermal reduction reaction

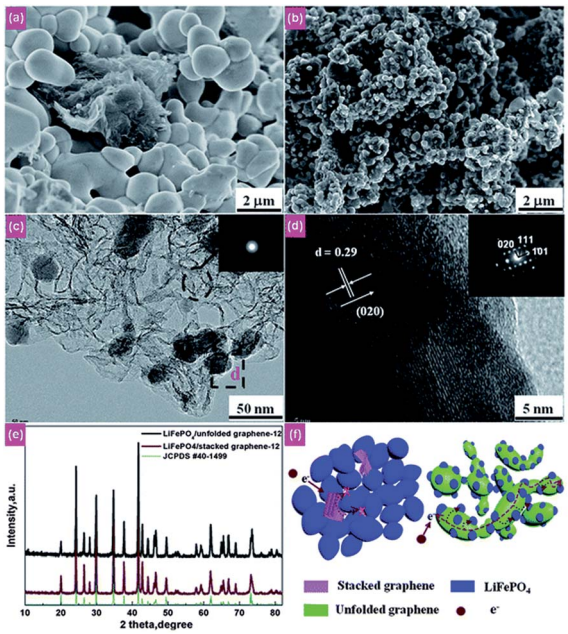

Fig. 2 SEM images of (a) stacked graphene/$LiFePO_4$ composites and (b) unfolded graphene/$LiFePO_4$ composites. (c) TEM image of $LiFePO_4$–unfolded graphene composites. (d) High-resolution TEM image and SAED pattern (inset) of an individual $LiFePO_4$ nanoparticle on unfolded graphene (square area in (c)). (e) XRD spectrum of the unfolded graphene/$LiFePO_4$ and stacked graphene/$LiFePO_4$ composites. (f) Electron-transfer pathway for the stacked graphene/$LiFePO_4$ and unfolded graphene/$LiFePO_4$ composites. Reproduced with permission from ref. 61. Copyright 2014, The Royal Society of Chemistry.

was also recently developed to synthesize a graphene/$LiFePO_4$ composite. The rheological approach can decrease the calcination temperature and save treatment time. Meanwhile, the sucrose pyrolysis produces an additional carbon coating on the $LiFePO_4$, improving the carbon conductive network for $LiFePO_4$.[74] More recently, an *in situ* pyrolysis and catalytic graphitization approach to synthesize graphene-decorated $LiFePO_4$ was developed.[75] Glucose and a trace amount of $FeSO_4$ were used as the graphene source and catalyst precursors, respectively. *Via* a solid state reaction, graphene formed a uniform coating layer on the $LiFePO_4$ nanoparticles. Because of the graphene conductive network, the obtained graphene–$LiFePO_4$ showed a superior specific capacity of 167.7 mA h g^{-1} and high rate performance with 94.3 mA h g^{-1} at 100 C.

Besides the dispersion and feasible synthetic methods, in the practical application of graphene in $LiFePO_4$, some other issues should be also considered. One is how to increase the interaction and bonding between $LiFePO_4$ and graphene. Encapsulating $LiFePO_4$ on graphene nanosheets with chemical bonding was recently achieved by a self-assembly method. Luo *et al.* modified $LiFePO_4$ particles by surface grafting aminopropyltrimethoxysilane to cover the surface with amino groups.[76] With the formation of peptide bonds between the amino groups on $LiFePO_4$ and the carboxyl groups on graphene, $LiFePO_4$ particles were successfully self-assembled on the graphene surface and formed a graphene oxide–encapsulated $LiFePO_4$ composite. With a subsequent reduction treatment, a graphene/$LiFePO_4$ composite with strong bonding and superior conductive network was formed, contributing to a high rate capability (70% capacity retention at 50 C) and excellent cycle performance (8.6% capacity loss after 950 cycles at 10 C). Another concern in the practical application of graphene with $LiFePO_4$ is lithium-ion diffusion rate through graphene. Despite $LiFePO_4$ conductivity being significantly improved with the addition of graphene, lithium ions may not easily pass through the carbon atom array of the 2D graphene sheets as expected. To favor lithium ion diffusion, modifying graphene sheets to produce more porosity allows rapid lithium ion diffusion, contributing to a high rate performance of $LiFePO_4$. For example, Ha *et al.* applied KOH activation to synthesize chemically activated graphene, which provided a porous continuous conductive network contributing to the superior electron transfer and fast lithium ion diffusion for $LiFePO_4$.[77]

Carbon nanotubes. In addition to graphene, carbon nanotubes are another widely studied carbon material. Because of their inherent network structure, carbon nanotubes are generally used for $LiFePO_4$ to form three-dimensional conductive networks, bridging the active particles. The incorporation of CNTs into $LiFePO_4$ has demonstrated enhanced capacity and rate performance for $LiFePO_4$.[78–80] When $LiFePO_4$ is combined with a CNT network, the conductive network facilitates charge mobility between the $LiFePO_4$ particles, contributing to the improved electrochemical performance of the entire $LiFePO_4$ electrode. By comparison, without an effective conductive network, charge distribution in the conventional C/$LiFePO_4$ electrode may be localized or trapped at grain boundaries inside the electrode, leading to local low performance.[81]

In most CNTs–$LiFePO_4$ composites, CNTs are randomly incorporated with $LiFePO_4$, which may not make full use of the CNTs conductive network because of the poor dispersion of CNTs in solution, owing to the high van der Waals forces.[82] Therefore, some functionalization methods have been developed on carbon nanotubes to improve the dispersion in $LiFePO_4$.[83,84] For example, poly(ethylene glycol) (PEG) was used to functionalize CNTs for $LiFePO_4$.[85] In addition to the improved dispersion of CNTs in $LiFePO_4$ particles, lithium-ion diffusion in a PEG-modified CNTs–$LiFePO_4$ electrode increased by two orders of magnitude, compared to the conventional $LiFePO_4$–acetylene black electrode.[88]

Another solution to avoid carbon nanotube aggregation is *via* the *in situ* growth of CNTs with $LiFePO_4$. Our group developed an *in situ* self-catalyzed formation of core–shell CNTs–$LiFePO_4$ nanowires (Fig. 3).[86] This novel composite was fabricated in two steps: a sol–gel route to form the one-dimensional $LiFePO_4$ precursor and a solid-state step to form core–shell CNT–$LiFePO_4$ nanowires. The CNT network was formed *via* the self-catalyzed reaction, where Fe^{2+} in the composite catalyzed the CNTs growth. The direct growth of CNTs from the composite effectively enhances the electronic conductivity. Meanwhile, the formation of CNTs also restricts the *in situ* crystallite growth of $LiFePO_4$ nanowires, thus controlling the nanowire size, which is important for the high rate performance of $LiFePO_4$. These 3D-CNT–$LiFePO_4$ nanowires delivered a capacity of 160 mA h g^{-1} at 17 mA g^{-1} and 65 mA h g^{-1} at 8500 mA g^{-1}.

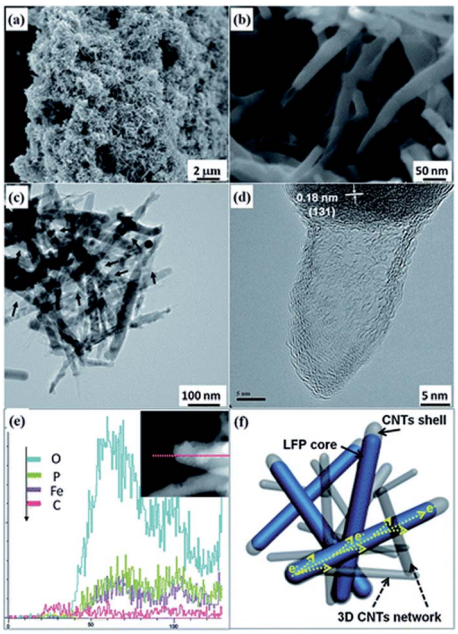

Fig. 3 (a and b) SEM images of the needle-like CNTs/$LiFePO_4$. (c) TEM image of the core–shell nanowires, and (d) the corresponding HRTEM image of a CNTs/$LiFePO_4$ nanowire. (e) EDX line profile of a CNTs/$LiFePO_4$ core–shell nanowire. (f) Schematic illustration of CNTs/$LiFePO_4$ core–shell nanowires. Reproduced with permission from ref. 86. Copyright 2014, The Royal Society of Chemistry.

In addition to graphene and carbon nanotubes, some other carbon structures have also been employed in $LiFePO_4$ composites. Mesoporous carbon materials with a hierarchical structure have high porosity, and thus may facilitate lithium-ion diffusion, shorten the diffusion paths, and increase the interfacial contact between electrolytes and $LiFePO_4$. Wang *et al.* developed a nanocasting technique to synthesize a mesoporous $LiFePO_4$/C nanocomposite.[87] The mesoporous structure improved the electronic/ionic contact, improved the mass and charge transfer capabilities, and delivered a high rate performance. Wu *et al.* developed another facile approach to obtain a mesoporous carbon nanosheet–$LiFePO_4$ composite *via* an *in situ* soft-template method.[88,89] The mesoporous carbon with high porosity served as both an electron and lithium-ion conductive network, contributing to an excellent rate capability. In spite of these superior performances, a feasible and low-cost synthesis route to the large-scale production of these advanced carbon materials, especially the porous carbon structure, is still very challenging for current battery material applications.

2.3. Morphology control

Decreasing the size of $LiFePO_4$ particles to the nanoscale enables higher power density, which is mainly attributed to the shortened ion diffusion pathways inside the 1D channels of $LiFePO_4$.[90,91] However, the size reduction also adversely affects the tap density and volumetric energy density, and the high surface area increases the undesirable electrode/electrolyte reactions, which leads to a poor cycling performance. Furthermore, unexpected antisite defects often accompany the size-reduction during $LiFePO_4$ synthesis.

Currently, morphology tailoring and controlled synthesis have attracted increased attention to improve the rate performance of $LiFePO_4$. In general, hydrothermal methods at low temperatures allow a well-controlled $LiFePO_4$ size and morphology, but the obtained material generally shows poor electrochemical performance because of the presence of antisite defects in the crystal structure.[92] The iron occupancy on the M1 site is considered to be an antisite defect, which blocks the lithium-ion diffusion pathway through the 1D channel along the (010) direction in the $LiFePO_4$ crystal structure, a process known as 'channel blocking'. The formation of these defects is due to the faster introduction rates of iron than lithium into the crystalline structure during the synthesis process. To guarantee an ideal crystalline structure for a high capacity, only when all the lithium is introduced into the crystalline structure will the defects be suppressed. To achieve this, some common strategies include extending the synthesis time, applying higher synthesis temperatures and applying post-treatment at high temperatures.[93] However, these methods also result in unexpected particle growth. Recently, it was found that the solvent plays an important role in controlling the antisite defects. Some solvents with low dielectric constants (such as ethylene glycol and ethanol) can reduce the concentration of Fe–Li antisite defects. For example, using ethanol as the sole solvent *via* a solvothermal process produced $LiFePO_4$/C that was highly crystalline and exhibited less than 1% antisite defects, and thus provides an alternative feasible route to limit the defects.[94]

In addition to suppressing the antisite defects, the orientation of $LiFePO_4$ particles tailored by morphology control also plays an important factor in improving the kinetics of the lithium-ion extraction/insertion process. The 1D lithium diffusion pathways along the (010) direction suggest that the synthesis of thin and well-dispersed $LiFePO_4$ nanostructures with a large (010) surface area would enhance its rate performance. Indeed, calculations based on the electronic structure of $LiFePO_4$ indicate that the low energy surfaces can dominate in the equilibrium shape.[95] Therefore, numerous efforts have been made to synthesize large surface area $LiFePO_4$ materials along their *b* axes to favor lithium ion diffusion.[96,97] It is well known that, at the thermodynamic equilibrium state, each facet's surface area in a crystal depends on its free surface energy.[98] However, the preference of crystal facets in $LiFePO_4$ is also linked with the properties of the solvent. Currently, most control of the $LiFePO_4$ (010) crystal facets are achieved with the solvothermal conditions, typically with ethylene glycol as the solvent.[99,100] The binding energy of a solvent, which is defined as the energy difference after the absorption of solvent molecules, is considered to play a decisive role in the facet control of $LiFePO_4$. A more recent report indicated that, when compared with ethylene glycol, the use of diethylene glycol is more favorable for (010) facet formation, due to the more stable binding geometry. The directional alignment of diethylene glycol molecules may take place at the (010) facet and produce a long chain, due to the hydrogen bonds between diethylene glycol molecules, thereby making the formed (010) surfaces

more stable. As a result, single-crystalline, (010)-oriented $LiFePO_4$ nanosheets (30–60 nm thick) were successfully synthesized by the solvothermal method with diethylene glycol solvent, as shown in Fig. 4.[101] With an ionic liquid solvothermal method, a controllable growth of the (010) facet of $LiFePO_4$ with high rate capability can be also obtained.[102]

Most conventional morphological control is based on a variety of nanostructures such as nanowires, nanoparticles, nanosheets and core–shell structures. In particular, the core–shell structured $LiFePO_4$/carbon composite allows fast lithium ion and electron transportation, enabling high electrochemical performance. For example, with an *in situ* polymerization method, Zhou *et al.* designed a $LiFePO_4$/carbon nanocomposite with a core–shell structure and the obtained $LiFePO_4$ showed a high rate capability and long life cycle.[103] In recent years, some new concepts have been introduced showing potential for future $LiFePO_4$ development. Quantum dots (QDs), tiny particles containing only a small number of atoms, have an extremely high surface-to-mass ratio. Because surface atoms generally possess a higher energy of delocalized electrons and are kinetically more active than interior atoms, QDs can generally exhibit superior properties. Recently, Zhang *et al.* synthesized high-energy quantum dots (HEQDs) in ultra-thin $LiFePO_4$ nanosheets.[104] It was found that the electrons and lithium ions can be easily transported to the HEQDs, due to its tunneling barrier, as shown in Fig. 5. This novel $LiFePO_4$ nanostructure provides more storage sites for lithium ions and shows a superior discharge capacity and an ultra-high coulombic efficiency. In recent years, atomic layer deposition (ALD) has attracted much attention as a novel technique to engineer nanostructures for energy materials. Owing to its unique capability to tune nanostructures at the atomic scale, our group recently successfully developed this technique to deposit $LiFePO_4$ on carbon nanotubes (CNT). The obtained $LiFePO_4$/CNT exhibited exceptional battery performance, including superior rate capability, power density and a long lifetime. The success of this technique in $LiFePO_4$ will also have a tremendous impact on future 3D all-solid state batteries and next-generation advanced battery systems (Fig. 6).[105]

In addition to the above fundamental issues, in practical applications, another big issue for lithium iron phosphate is related to the tap density. The large-scale industrial application of lithium-ion batteries in electric vehicles not only requires a high specific capacity, but also a high tap density of $LiFePO_4$ which means a high volumetric energy density.[106,107] To meet the requirement of high tap density but to maintain all the merits of nanosized materials, porous $LiFePO_4$ microspheres with interconnected open pores are advantageous, because this can reduce the diffusion length of lithium ions, facilitating fast lithium ions diffusion.[108–110] Carbon-coated $LiFePO_4$ microspheres with high tap densities can be synthesized by co-precipitation, hydrothermal and solvothermal methods. The fundamental understanding of the seed nucleation, growth, precipitation and some other factors (*e.g.* chemical potential, the choice of solvent and surfactant addition), as well as the development of a simple, feasible and low-cost synthetic route, is still critical for the future of $LiFePO_4$.[111,112] Nanosized $LiFePO_4$, generally synthesized by low-temperature solution routes, is susceptible to the presence of some defects due to the turbostratic stacking of the layers, which leads to perturbation of the lattice and localized charge at the external surface and in the 1D channels, limiting lithium ion diffusion. In contrast, large-sized crystals with a less disordered

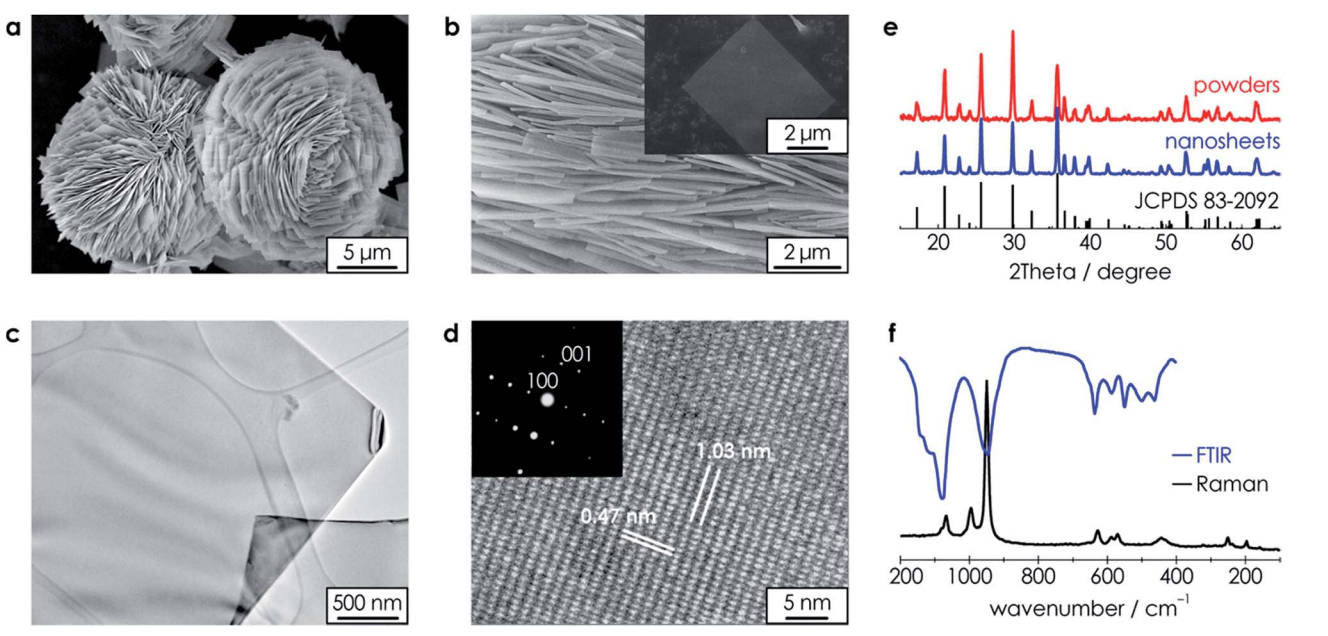

Fig. 4 Characterization of $LiFePO_4$ nanosheets. (a) Representative SEM image of $LiFePO_4$ particles; (b) SEM image of the accumulated nanosheets. Insert: an individual exfoliated $LiFePO_4$ nanosheet. (c) TEM and (d) HRTEM image and ED pattern of the $LiFePO_4$ nanosheets. (e) XRD patterns of $LiFePO_4$ particles and exfoliated $LiFePO_4$ nanosheets. (f) Raman (black) and FTIR (blue) spectra of the as-exfoliated $LiFePO_4$ nanosheets. Reproduced with permission from ref. 101. Copyright 2014, American Chemical Society.

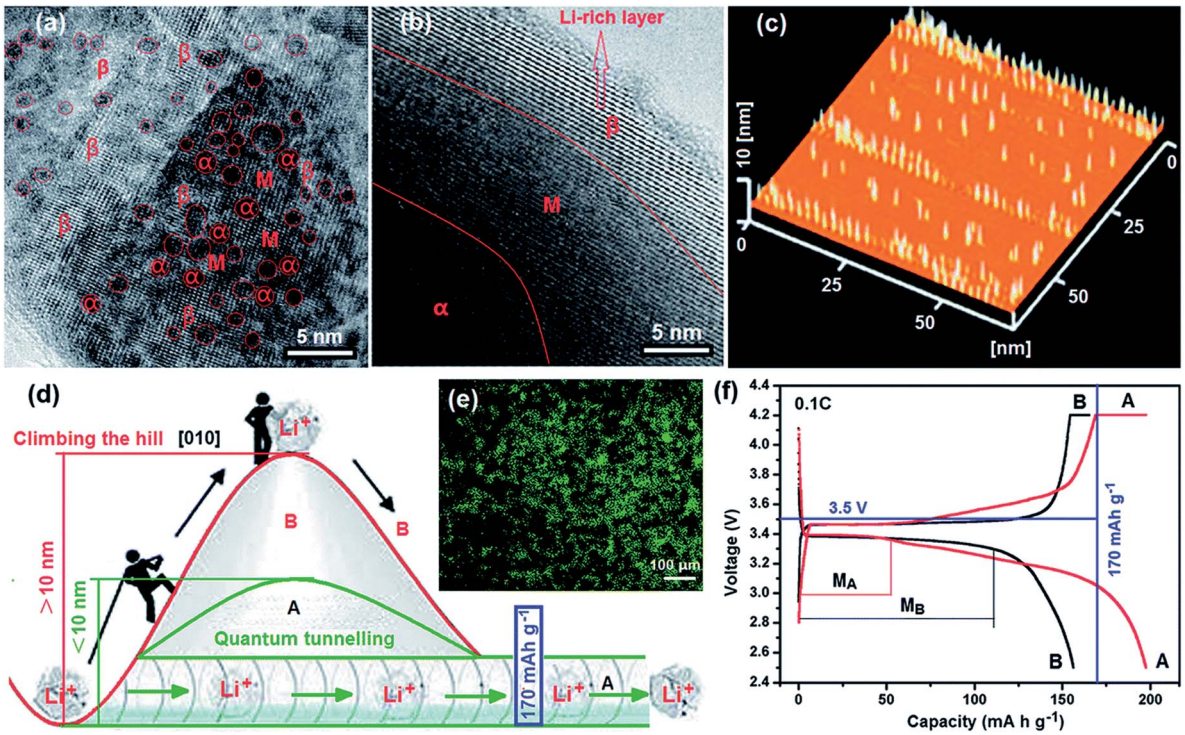

Fig. 5 Characterizations of high-energy $LiFePO_4$ quantum dots (HEQDs). (a) HRTEM image of HEQDs embedded in a $LiFePO_4$ nanosheet. (b) HRTEM image of a commercial $LiFePO_4$ particle. (c) AFM image of the size and height distributions of HEQDs embedded in a $LiFePO_4$ nanosheet. (d) Li ion pathways in the commercial sample (B) and mesoporous biocarbon nanowire coated $LiFePO_4$ (MBCNW–LFP–HEQDs) (A). (e) Fluorescent image of MBCNW–LFP–HEQD-2 sample, (f) the first discharge/charge curves of MBCNW–LFP–HEQD-2 cathode (A) and the commercial cathode (B) at 0.1 C rate. Reproduced with permission from ref. 104. Copyright 2014, The Royal Society of Chemistry.

arrangement allow undisturbed paths for lithium-ion diffusion. The delithiation process is considered to occur near the surface in a large $LiFePO_4$ crystal; however, it is preferable to take place at the core of a small crystal.[113] In addition, large $LiFePO_4$ particles with high tap densities seem to exhibit a higher degree of electrochemical reversibility. Previous studies indicate some difference in the delithiation behavior between large and small single crystals.[114,115] Based on the above discussion, it is critical to optimize the synthesis conditions to produce well-ordered $LiFePO_4$ crystals with a suitable size (not solely focusing on nanosized crystals), high tap density, few defects and high reversibility.

2.4. Element doping

In addition to carbon coating and morphology/size control strategies, doping is considered to be another significant method to enhance the intrinsic electronic/ionic conductivity of $LiFePO_4$. In particular, considering the limiting factor for the rate performance is due to the poor lithium-ion diffusion, substitution of a small amount of Li^+, Fe^{2+} or O^{2-} by other ions is expected to enhance the charge/discharge property at high current densities. Although the role of doping in $LiFePO_4$ is still unclear and under debate, doped $LiFePO_4$ indeed has exhibited improved electrochemical performance in numerous studies.

Lithium site doping. The first work about Li site doping was reported by Chung *et al.*, stating that a significant increase in $LiFePO_4$ electronic conductivity by around 8 orders of magnitude was achieved to reach 10^{-2} S cm^{-1} with a low amount of dopant (Mg, Zr, and Nb, no more than 1 at% at Li M1 site).[116] The dramatic increase in conductivity was later attributed to carbon coating and the metallic iron phosphides/carbophosphides on the $LiFePO_4$ surface during the solid state reaction process at high temperatures (above 700 °C).[117,118] Since then, the possibility and practical role of Li site doping has aroused enormous research interest.

From conventional wisdom, lithium ions diffuse along 1D tunnels in $LiFePO_4$, and the presence of immobile dopants at the Li site may impede lithium-ion diffusion, which should result in a low rate performance for $LiFePO_4$. Nazar recently revisited this topic by using neutron and X-ray diffraction for aliovalent cation-doped $LiFePO_4$ with Zr, Nb and Cr doping elements.[119] The result confirms that these dopants indeed exist on Li M1 sites with ~3 atom% substitution after a solid-state reaction at 600 °C. However, these dopants cannot significantly affect lithium-ion diffusion in $LiFePO_4$ because the lithium-ion diffusion channels are only increased 0.3% by these dopants. Instead, these immobile dopants residing within lithium-ion channels certainly will hinder lithium-ion diffusion, resulting in lower rate performance. Nevertheless, some experimental reports indicate that Li site doping indeed enhances the rate performance of $LiFePO_4$.[120,121] So far, the true role and effects of Li doping for $LiFePO_4$ electrochemical performance has still not been fully ascertained and remains controversial.

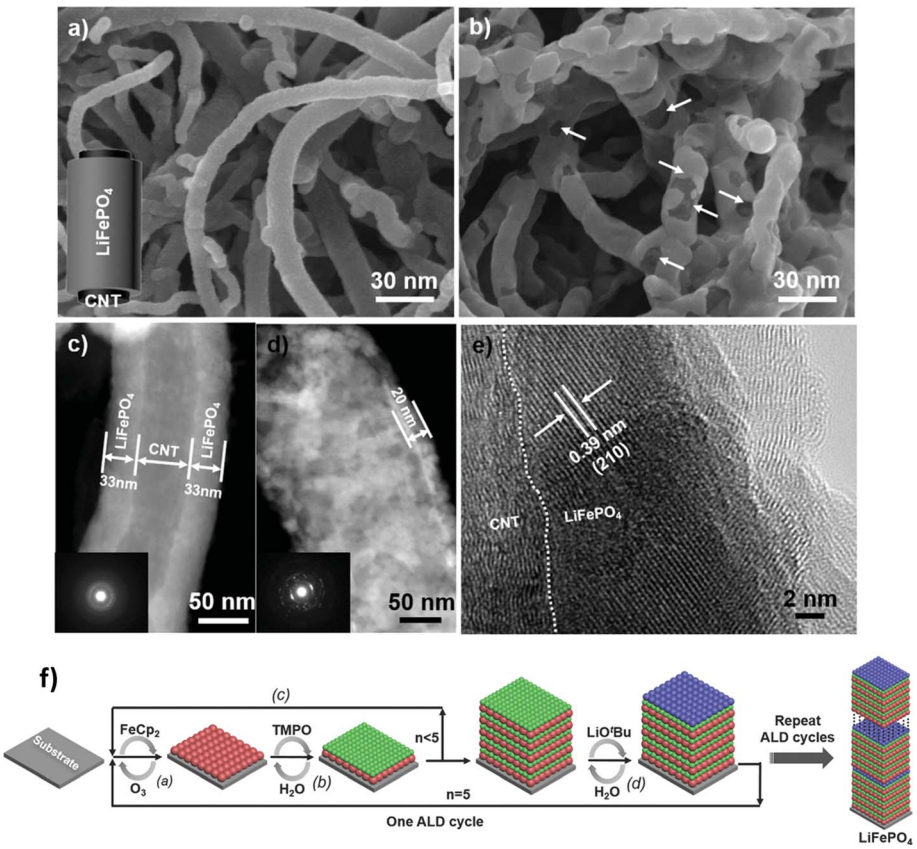

Fig. 6 SEM images of (a) as-prepared CNTs/$LiFePO_4$ and (b) annealed CNTs/$LiFePO_4$. Scanning transmission electron microscopy images of (c) as-prepared CNTs/$LiFePO_4$ and (d) annealed CNTs/$LiFePO_4$. (e) HRTEM image of the annealed CNTs/$LiFePO_4$. (f) Schematic illustration showing the ALD principle for the synthesis of $LiFePO_4$. Reproduced with permission from ref. 105. Copyright 2014, WILEY-VCH Verlag GmbH & Co. KGaA.

Iron site doping. In comparison to Li site doping, more researchers have performed substitution (aliovalent and isovalent) at the Fe (M2) site. Similar to the debates on Li site doping, the feasibility and roles of Fe site doping, especially aliovalent doping, is still under debate. Using an atomistic simulation method, Islam *et al.* previously suggested that only divalent metal elements can be doped in the $LiFePO_4$ lattice, but aliovalent doping was not successful.[122] However, many publications report the improved electrochemical performance of $LiFePO_4$ with aliovalent doping (*e.g.* Mo^{6+}, Ti^{4+}, V^{5+}, Nb^{5+}).[123–126] From these reported studies, aliovalent doping seems to be feasible and its beneficial role in $LiFePO_4$ electrochemical performance indeed exists. The remaining question is what exactly contributes to this improvement, and this has been the research focus for doped $LiFePO_4$.

Among those aliovalent doping elements, vanadium has become one of the most interesting dopants in recent years, due to its various oxidation states and coordination chemistry. Vanadium also can form electrochemically active phases (*e.g.* $Li_3V_2(PO_4)_3$, $LiVOPO_4$ and V_xO_y) and its use can avoid inactive impurity substances in lithium-ion batteries. Therefore, some recent studies selected vanadium as a model dopant to investigate why aliovalent doping in Fe site can increase the rate of lithium removal/insertion in $LiFePO_4$.[127–129] X-ray diffraction indicates that vanadium-doped $LiFePO_4$ at an Fe site can reduce the lattice mismatch between Li-rich and Li-poor phases. It also increases the composition width of the single phase (solid solution range), which is beneficial for the fast charge/discharge ability. In addition, V-doped $LiFePO_4$ shows a lower single-phase transformation temperature.[130] Combining X-ray with neutron powder diffraction methods, Whittingham's group recently confirmed that the doped aliovalent vanadium indeed occupy Fe sites, but some Fe exist at Li sites, which increases the unit cell volume.[131] Similar to the previous report, this aliovalent doping may reduce the miscibility gap and the solid solution formation temperature, which contributes to the high rate performance. However, this V doping and some Fe residing at Li sites also significantly decrease the capacity of $LiFePO_4$ at moderate temperatures. Therefore, the control of proper doping at preferable sites is important for the overall $LiFePO_4$ performance improvement.

In terms of the doping process, the elemental doping involves many factors, including temperature, time, precursors and the $LiFePO_4$ itself. In general, a low ratio of aliovalent ions doping (less than 10 mol%) at the Fe site can be achieved by conventional solid state methods, but a higher degree of doping needs novel synthetic routes. With a microwave-assisted synthesis process, Harrison recently reported an aliovalent

doping with up to 20% V substitution at Fe sites.[132] The temperature dependence of V doping in $LiFePO_4$ was also confirmed. Nevertheless, further studies and optimization of the doping experimental parameters are still needed.

Compared with aliovalent doping, isovalent substitution is more normal in nature for $LiFePO_4$, and many divalent cations (*e.g.* Mn, Co, Ni, and Mg) were doped at the Fe site with a high doping degree, and showed enhanced electrochemical performance.[133–136] Among the isovalent cations, Mg^{2+} doping is most often reported to improve the electrochemical kinetics of $LiFePO_4$. From the first-principles density-functional theory, Mg doping prefers to reside at the Fe site rather than Li site, leading to high lithium-ion diffusion.[137] By using X-ray diffraction for a partially (de)lithiated $LiMg_{0.2}Fe_{0.8}PO_4$ sample, a recent study indicates the existence of stable equilibrium intermediate phases (Fig. 7).[138] As a result, the Mg-doped $LiFePO_4$ may undergo a single-phase process during the lithiation/delithiation process, which may play a significant role in improving the electrochemical performance of Mg-doped $LiFePO_4$. In addition, the formation energies and the cell volumes decreased gradually with the increase in Mg concentration in Mg-doped $LiFePO_4$, which also enhance the lithium-ion diffusion rate in $LiFePO_4$.[137]

Isovalent Mg doping at Fe sites can enhance the electronic conductivity and electrochemical activity for $LiFePO_4$. However, that is not the case if the isovalent Mg doping occurs at Li sites. Mg-doped $LiFePO_4$ is size-dependent in terms of electrochemical performance.[139] Compared with Fe site doping, Mg doped at the Li site exhibits a low capacity and poor electrochemical kinetics, due to blocking effect by Mg on the lithium-ion diffusion path. Interestingly, this adverse effect may be diminished after long-term electrochemical cycles, which may be due to the gradual ion exchange between Mg ions and Li ions.

In addition to the above Li and Fe site doping, anion doping at the O site was also reported to improve the electrochemical performance, such as the cycle and rate capabilities. These doped anions include Cl, F and Na.[140,141] However, compared to the extensively studied Fe and Li doping, O site doping has been less studied and is seldom used. There are limited references and resource available. Therefore, no detailed discussion about this topic is presented in this review.

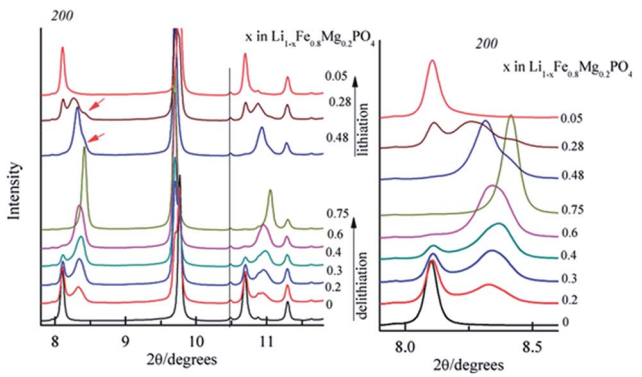

Fig. 7 High-resolution XRD patterns of $LiMg_{0.2}Fe_{0.8}PO_4$ at different states of charge/discharge. Upon lithiation to $x = 0.48$, two phases are observed. One is the lithium-poor phase (a hump as shown by the arrow) and the other is the intermediate phase. Reproduced with permission from ref. 138. Copyright 2014, WILEY-VCH Verlag GmbH & Co. KGaA.

3. Delithiation and lithiation mechanisms

Understanding the phase transformation mechanism and the lithium intercalation pathway in $LiFePO_4$ is of crucial importance, because the intercalation kinetics directly determines the capacity, rate performance and columbic efficiency. In terms of the phase transition mechanism, it is generally accepted that $LiFePO_4$ undergoes a typical first-order phase transformation, with nucleation and growth of the second phase during the lithium extraction/insertion process, leading to a two-phase equilibrium composed of a Li-poor Li_xFePO_4 phase and a Li rich $Li_{1-y}FePO_4$ phase, which gives a stable voltage plateau at ~3.5 V.[142] The unit-cell volumes of both phases remain nearly constant, with the unit cell volumes of the two phases varying by only $\Delta V = 6.5\%$.[143] The small volume change during the phase transformation contributes to the unique advantages of $LiFePO_4$, namely superior structural stability and safety, making it an ideal battery material for electric vehicle applications. Although many studies support the two-phase mechanism of $LiFePO_4/FePO_4$, the specific model still remains controversial, including the core–shell,[1,144] domino cascade,[145] spinodal decomposition,[146,147] and mosaic mode[148] *etc.* (Fig. 8 and Table 1). Because the delithiation/lithiation kinetics and phase compositions strongly depend on the particle size, morphology and physical properties of the studied $LiFePO_4$ material, the above disagreement, and even the conflicting models, may be attributed to the specific experimental conditions.

In recent years, with the advancement of microscopic and spectroscopic experimental techniques, a solid solution reaction and intermediate phase have been detected in $LiFePO_4$,[149,150] which also provide another possible phase transformation mechanism for $LiFePO_4$. In general, under a typical solid solution reaction for most materials, the lattice parameters and unit-cell volumes change continuously during the phase transformation process. As in the case of $LiFePO_4$, the solid-solution process and possible intermediate phase have been detected at different extreme experimental conditions, such as with very tiny particle sizes (tens of nanometers) or ultra-high charging rates (over 10 C) *via* some *in situ* or *in operando* characterization methods.[151,152]

In addition, the recent research interest on $LiFePO_4$ phase transformation mechanism has been extended from a single-particle to a multi-particle system, as well as to the entire electrode behavior,.[153,154] In the case of real $LiFePO_4$ electrodes, there is an assembly of a large amount of active $LiFePO_4$ particles with possible differences in inhomogeneity, thickness and porosity. In this section, we will overview some recent understanding and findings on this hotly debated subject of the $LiFePO_4$ phase transformation mechanism.

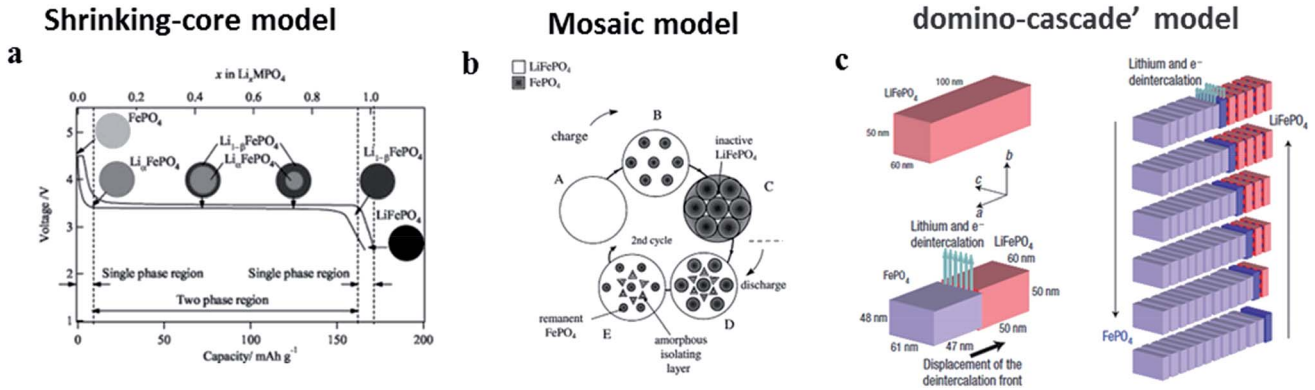

Fig. 8 Several classic two-phase models for $LiFePO_4$. (a) Shrinking-core model, reproduced with permission from ref. 144. Copyright 2005, The Electrochemical Society. (b) Mosaic model, reproduced with permission of ref. 148. Copyright 2001, Elsevier. (c) Domino-cascade model, reproduced with permission of ref. 145. Copyright 2008, Nature Publishing Group.

Table 1 Two-phase models in single-particle $LiFePO_4$ system

Mechanism	Sample size/ morphology	Characterization tools	Experimental method	Ref.
Core–shell	Micrometric particles	X-ray diffraction	Chemical/electrochemical delithiation	1
Shrinking-core	100–200 nm nanoparticles	Mathematical model	Electrochemical delithiation	18
Radial model	140 nm nanoparticles	High-resolution electron energy loss spectroscopy	Electrochemical delithiation	10
Spinodal model	100 nm nanoparticles	Raman and high-resolution transmission electron microscopy	Electrochemical delithiation	146 and 147
Mosaic model	Solid state route	Neutron powder diffraction	Electrochemical delithiation	148
Domino-cascade model	100 nm nanoparticles	XRD and HRTEM	Electrochemical delithiation	145
Two-phase coexistence	Micrometric LFP particle	*In operando* transmission X-ray microscopy	Electrochemical delithiation	159
Two-phase coexistence	Micrometric single crystals	Transmission X-ray microscopy	Chemical delithiation	157

3.1. Two phase coexistence

The well-known two phase mechanism in $LiFePO_4$ has two explanations, that is, intra-particle and inter-particle two-phase coexistence. Some studies suggest that the two-phase coexistence only occurs in the inter-particle system, that is to say, all the individual $LiFePO_4$ particles are either completely delithiated ($FePO_4$) or lithiated ($LiFePO_4$).[155,156] This explanation has been supported by recent *ex situ* work *via* Transmission Electron Microscopy (TEM) and X-ray Microscopy (soft and hard X-ray technology).[157,158] However, this two-phase coexistence may change with particle size, morphology and the electrochemical testing conditions (fast or slow charging rate, static or dynamic, *etc.*). Recent work using hard X-ray microscopy to track $LiFePO_4$ phase transformation under *in operando* conditions reveals two-phase coexistence in individual microsized $LiFePO_4$.[159] The microscale-sized $LiFePO_4$ is not robust, so the large mismatch between the two end members may lead to energy relaxation, as revealed by the formation of cracks or structural dislocations but not sufficient to drive the fast phase transformation. The weak driving force only allows boundary displacement to occur at the surface-near sites, resulting in the two-phase coexistence in the individual large particles.[160,161] In contrast, as for nanosized $LiFePO_4$, the large mismatch and local constraints between the two end members drive fast boundary displacement, allowing the fast phase transformation reaction. As a result, the nanosized $LiFePO_4$ is more susceptible to exhibit either full delithiation ($FePO_4$) or full lithiation ($LiFePO_4$). Therefore, the size effect plays an important role in the intra-particle delithiation mechanism for $LiFePO_4$ (Fig. 9).[159]

3.2. Solid-solution mechanism

Although the two-phase mechanism has been widely accepted and the presence of the two-phase transformation in $LiFePO_4$ is generally considered to limit its fast charging performance, in practice, $LiFePO_4$ batteries have been successfully commercialized and applied in electric vehicles, demonstrating high rate performance. The contradiction between the theoretically low ion-diffusion capability and practically high-rate capability

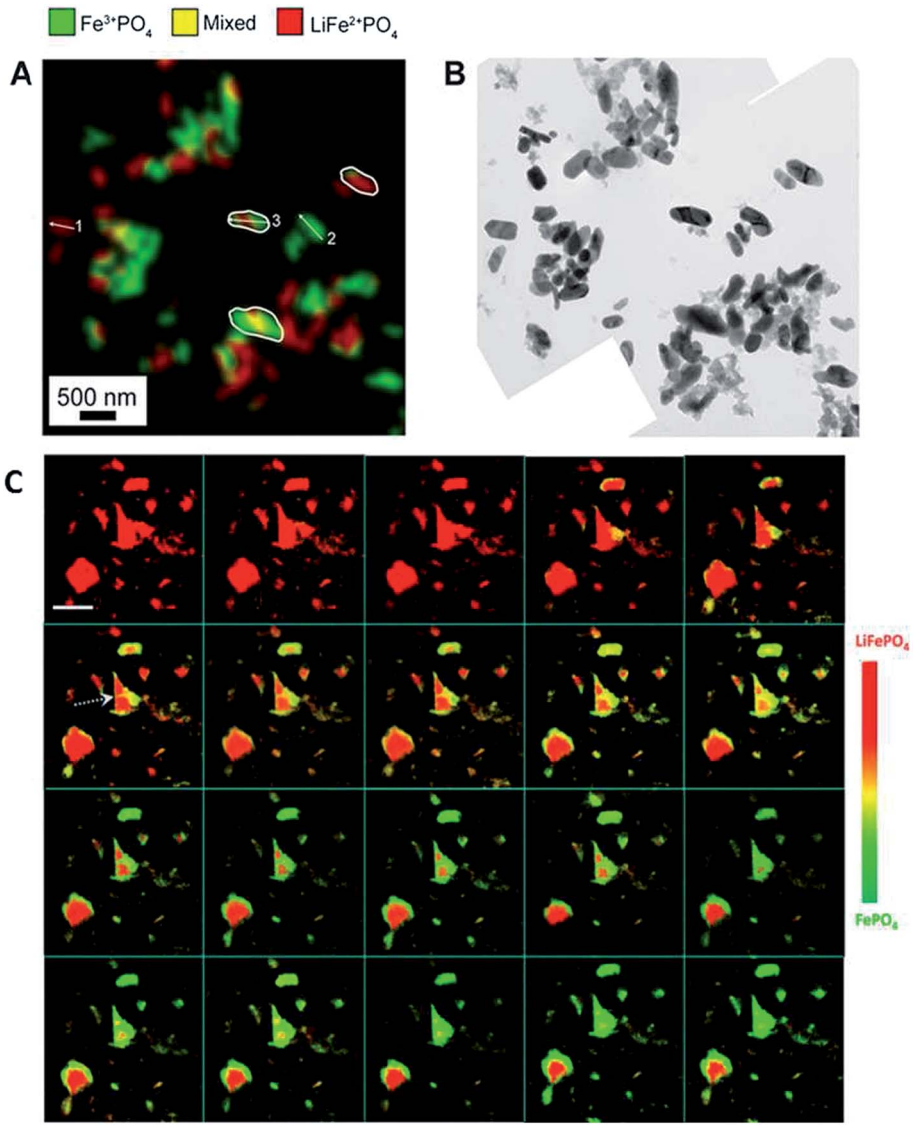

Fig. 9 X-ray chemical mapping of two-phase coexistence in inter-particle ((A) soft X-ray imaging of partially charged $LiFePO_4$; (B) the corresponding TEM image from an *ex situ* experiment) and intra-particle ((C) *in operando* hard X-ray imaging experiment). The dashed arrows reveal crack formation in some individual particles in (C). Scale bar is 10 μm in C. Reproduced with permission from ref. 158 and 159. Copyright 2013 American Chemical Society (a and b) and 2014 Nature Publishing Group (c).

pushes us to revisit the two-phase mechanism in $LiFePO_4$. Indeed, some previous theoretical research suggests that the miscibility gap between the two end members may decrease or even disappear, but most of the assumptions are only effective under extreme conditions, such as using extremely small particles (below 15 nm)[162] or high temperatures (~350 °C),[163] which cannot completely explain the high rate performance for true $LiFePO_4$ batteries under practical working conditions (*i.e.* room temperature, hundreds of nanoscales or microscale). As a result, a nonequilibrium solid solution may occur and play a critical role in the observed high rate capability of $LiFePO_4$ electrodes. In recent years, with the advancement of characterization tools and the use of *in situ* or *in operando* methods, an increasing amount of experimental evidence validates this assumption.

Based on some theoretical methods, such as first-principles and phase-field modeling, a solid-solution mechanism has been previously proposed,[164,165] which suggest the phase transformation between $LiFePO_4$ and $FePO_4$ may undergo a single-phase, not two-phase mechanism. Recent research suggests that the phase separation is able to be suppressed in the nominally two-phase region, especially for nanosized particle at high rates. This was supported by experimental results, as a long-range lithium-ordered $Li_{0.5}FePO_4$ phase in half-delithiated $LiFePO_4$ single-crystalline nanowires was shown with TEM.[166] A continuous shift of the diffraction peaks was also shown during the lithium insertion/extraction process for a $LiFePO_4$ nanoparticle (40 nm) at room temperature.[167] These experimental findings obviously support the above assumption.

Since the realization of the solid-solution phases, there arises another debate about the width, form and role of a solid-solution zone during battery charging and discharging. Although the solid-solution mechanism has been confirmed, many reported experimental results and conclusions are inconsistent, including an atomically sharp interface,[168] a 4 nm disordered interface,[160,169] and a long-range ordered structure in partially delithiated $LiFePO_4$.[170,171] For example, for this staging structure (a pronounced long-range order), a recent study indicates a size-dependent behavior. As to the small crystals, staging exists in the whole particle with a decrease of order from the center to the surface. For the larger crystal, an intermediate phase appears between $LiFePO_4$ and $FePO_4$, and the staging interfacial width changes little with the size increase.[172] In addition to the size-dependency, the solid-solution phase transformation in $LiFePO_4$ is also found to be rate dependent. At high rates, such as over 10 C, the solubility limits in both phases increase dramatically, leading to a fraction of the electrode material following a single phase transformation path, bypassing the first-order phase transition.[173] Obviously, the topic continues to be debated and more fundamental studies and direct experimental evidence are thus needed.

The convincing evidence for the solid-solution mechanism is a direct characterization of this solid-solution zone under *in situ* or *in operando* conditions. Previous theoretical calculations have shown that this solid-solution zone is thermodynamically metastable.[174] Using *in situ* high-resolution TEM, Niu *et al.* recently observed a disordered Li-sublattice solid-solution zone (10–25 nm × 20–40 nm in size). Different from the sharp interface in other *ex situ* studies, the observed wide solid-solution zone shows no dislocations, which is considered to contribute to the high rate performance of $LiFePO_4$. In addition, it also suggests that this disordered solid-solution zone could dominate the phase transformation process, even at high charging rates. This dynamic observation provides a more accurate understanding of the solid-solution zone (Fig. 10).[175]

Further experimental evidence was also obtained *via* an *in situ* synchrotron X-ray study. Because of the high sensitivity, time resolution and accuracy,[176–178] synchrotron X-ray diffraction is the most suitable technique to detect the possible intermediate phase under charging and discharging of $LiFePO_4$. With the *in operando* XRD technique, Orikasa *et al.*[179] tracked the phase transformation process and found a metastable crystal phase in fast-charging microsized $LiFePO_4$, in addition to the thermodynamically stable $LiFePO_4$ and $FePO_4$ phases (Fig. 11). Also, it was found that this metastable phase has a short life time (a couple of minutes), as it diminishes under open-circuit conditions. This metastable Li_xFePO_4 (x = 0.6–0.75) only appears at high charging rates, and is absent at slow charging rates in the $LiFePO_4$ electrode. Therefore, it is suggested that at high rates, the phase transformation in $LiFePO_4$ may pass through the metastable phase, which decreases the nucleation energy and thus leads to a higher rate performance for the $LiFePO_4$. Another of the latest *in situ* XRD studies captured the metastable solid-solution phase in fast-charging nanosized $LiFePO_4$ (Fig. 12).[180] Different from the intermediate Li_xFePO_4 (x = 0.6–0.75) phase at high rates in the microsized samples, the studies with nanosized $LiFePO_4$ demonstrate the

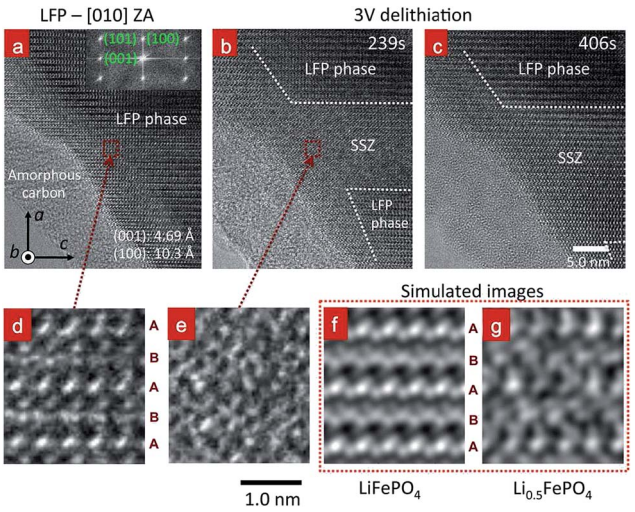

Fig. 10 *In Situ* TEM study of the delithiation process of a $LiFePO_4$ crystal viewed from [010] axis (a–c). (a) The $LiFePO_4$ showing a clear crystal structure before voltage applied. (b) A clear solid solution zone (SSZ) and a directional boundary propagation were observed at 239 s. (c) the images of the SSZ and boundary evolution at 406 s. (d and e) The magnified images of the selected regions in (a and b), respectively. The simulated TEM images of (f) $LiFePO_4$ and (g) $Li_{0.5}FePO_4$. Reproduced with permission from ref. 175. Copyright 2014 American Chemical Society.

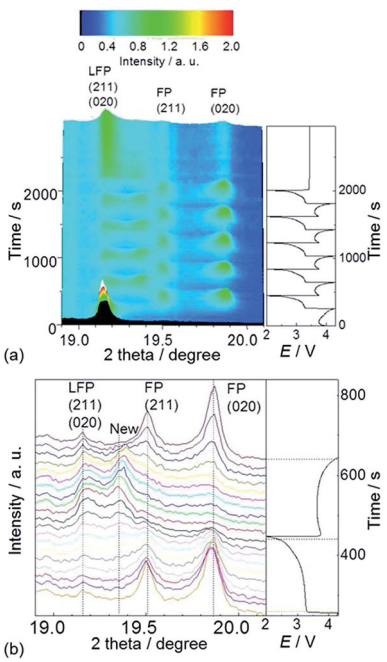

Fig. 11 *In situ* synchrotron XRD study of $LiFePO_4$ under electrochemical cycles. (a) Time-resolved XRD patterns for $LiFePO_4$ during charge–discharge cycles at 10 C rate. (b) Detailed XRD patterns during the first discharge and second charge cycles. A new peak at 19.35° was formed during cycling. Reproduced with permission from ref. 179. Copyright 2013 American Chemical Society.

continuous solid-solution phase has a wide composition, Li_xFePO_4 ($0 < x < 1$). This is composed of the entire range between the two end members of $LiFePO_4$ and $FePO_4$ at high rates. This suggests that nanosized $LiFePO_4$ may undergo continuous structural change without the phase boundary movement and nucleation step, which also helps explain the high rate performance of $LiFePO_4$.

Furthermore, the (de)lithiation mechanism and solid-solution formation is also related to the type of olivine lithium phosphate. A typical example is lithium manganese iron phosphate (LMFP), a very promising cathode material with a higher working voltage and similar structural stability.[181,182] Recently, *in operando* synchrotron XRD indicated that, in contrast to $LiFePO_4$, nano-LMFP exhibits a continuous solid-solution process, which can be observed at a wide composition range. The dominant metastable solid-solution process occurring at LMFP can explain the higher rate capacity than for $LiFePO_4$ with comparable particle sizes, in spite of a larger volume misfit (11.6% for $LiMnPO_4$, 6.5% for $LiFePO_4$).[183]

A similar report from Whittingham's group also indicated that Li(Mg, Mn, Fe)PO_4 undergoes a one-phase (de)lithiation mechanism. Mg substitution in the mixed olivine, $LiFe_{0.6}Mn_{0.4}PO_4$, reduces the lattice misfit between the two end-member phases. This smaller lattice mismatch and the interactive forces (Mn, Fe and Mg) result in a one-phase (de)lithiation mechanism.[184]

The (de)lithiation mechanism is also related to the $LiFePO_4$ structure. Recently, a novel non-olivine $LiFePO_4$ with an alluaudite structure was successfully developed.[185] In contrast to the two-phase reaction in olivine $LiFePO_4$, the alluaudite $LiFePO_4$ showed fundamentally different electrochemical behavior. In spite of the similar Fe^{2+}/Fe^{3+} redox reaction, the alluaudite $LiFePO_4$ showed a one-phase reaction mechanism, allowing fast lithium ion diffusion. The fast charging property is

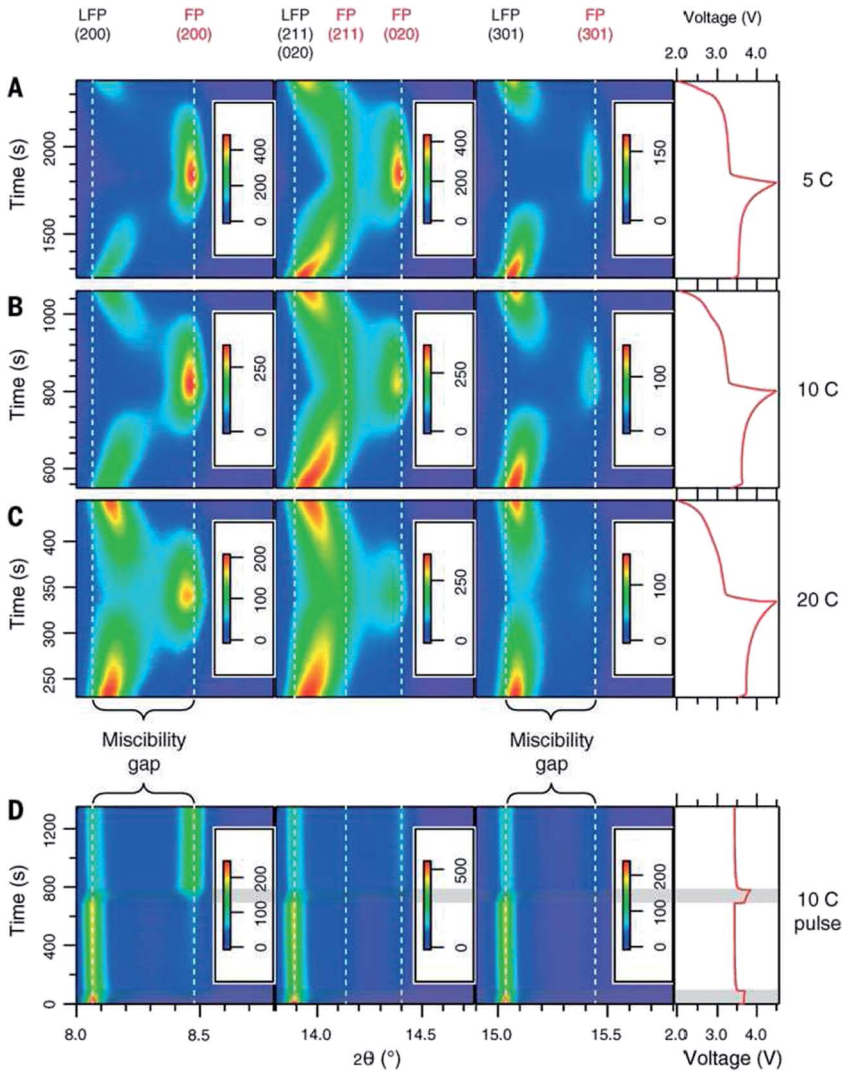

Fig. 12 *In situ* XRD study of $LiFePO_4$ under different electrochemical cycles. (A–C) patterns of the second galvanostatic cycle at 5, 10, and 20 C, respectively. (D) Patterns of the evolution of the charge-relax experiment, where a 10 C current is applied for 90 s followed by an open-circuit relaxation of 10 min. Reproduced with permission from ref. 180. Copyright 2014, the American Association for the Advancement of Science (AAAS).

attributed to the unique structure of the alluaudite. An alluaudite compound has the formula $X(1)X(2)M(1)M(2)_2(PO_4)_3$ and the structure contains edge sharing $M(2)O_6$ octahedra chains, connected by distorted $M(1)O_6$ octahedra. X(1) and Li in the targeted structure occupy the X(2) site, and Fe occupies the M(1) and M(2) sites. Tetrahedral PO_4 units connect the chains, and X cations reside in tunnels along the *c*-axis, providing possible diffusion pathways. Although this novel structured $LiFePO_4$ enhances the fast charging performance *via* a one-phase mechanism, many issues related to the alluaudite structure are still unclear, such as the thermal stability and electronic conductivity. Also, only around 0.8 lithium ions could be delithiated and reversed back in the one-phase reaction. The specific capacity and cycle performance are unsatisfactory. Further studies are still needed.

In addition to the proposed two-phase and solid-solution mechanisms, a mixed mechanism has also recently been suggested. With *in operando* synchrotron high-energy X-ray diffraction (XRD), nonequilibrium lithium insertion and extraction from the $LiFePO_4$ cathode was studied. Neither the $LiFePO_4$ phase nor the $FePO_4$ phase maintained a static composition during lithium insertion/extraction.[186] Instead, the $LiFePO_4$ cathode simultaneously experienced both a two-phase reaction mechanism and a dual-phase solid-solution reaction mechanism over the entire range of the flat voltage plateau, with this dual-phase solid-solution behavior being strongly dependent on the charge/discharge rates. The proposed dual-phase solid-solution mechanism may explain the remarkable rate capability of $LiFePO_4$ in commercial cells. A similar mechanism was also reported by *in situ* neutron powder diffraction and a simultaneous occurrence of solid-solution and two-phase reactions after deep discharge under nonequilibrium conditions was suggested (Fig. 13 and Table 2).[187]

3.3. Multi-particle system

Since numerous studies of the (de)lithiation mechanism are based on individual $LiFePO_4$ particles, a full understanding of the entire electrode behavior is still not clear. This is because the mechanism in a single-particle $LiFePO_4$ system may not necessarily be suitable for an entire electrode, considering the issues arising from the thickness, inhomogeneity, porosity and particle overlapping. Recent research has suggested that in an electrode assembly, all $LiFePO_4$ particles are not (de)lithated simultaneously but rather sequentially *via* a particle-by-particle intercalation pathway.[188] That is to say, in contrast to the "concurrent" mechanism, two-phases coexist in the inter-particle at the entire electrode, which is considered to be due to the fast inter-particle transport, the quick phase boundary replacement and the decrease of interfacial energy.[189]

The inhomogeneous $LiFePO_4/FePO_4$ phase distribution at the entire-electrode scale was confirmed by *ex situ* Scanning Transmission Electron Microscopy (STEM).[190] At the mesoscale, a core–shell phase distribution with a preferential pathway along the porosities was found. At a larger scale, the (de)lithiation process occurs *via* a "stratum-by-stratum" pathway, from the electrolyte side to the current collector. It is obvious that the electrochemical reaction is more favorable to occur at some electrolyte-accessible sites with more porosity, as lithium-ion diffusion is one of the main limiting factors. Another study with

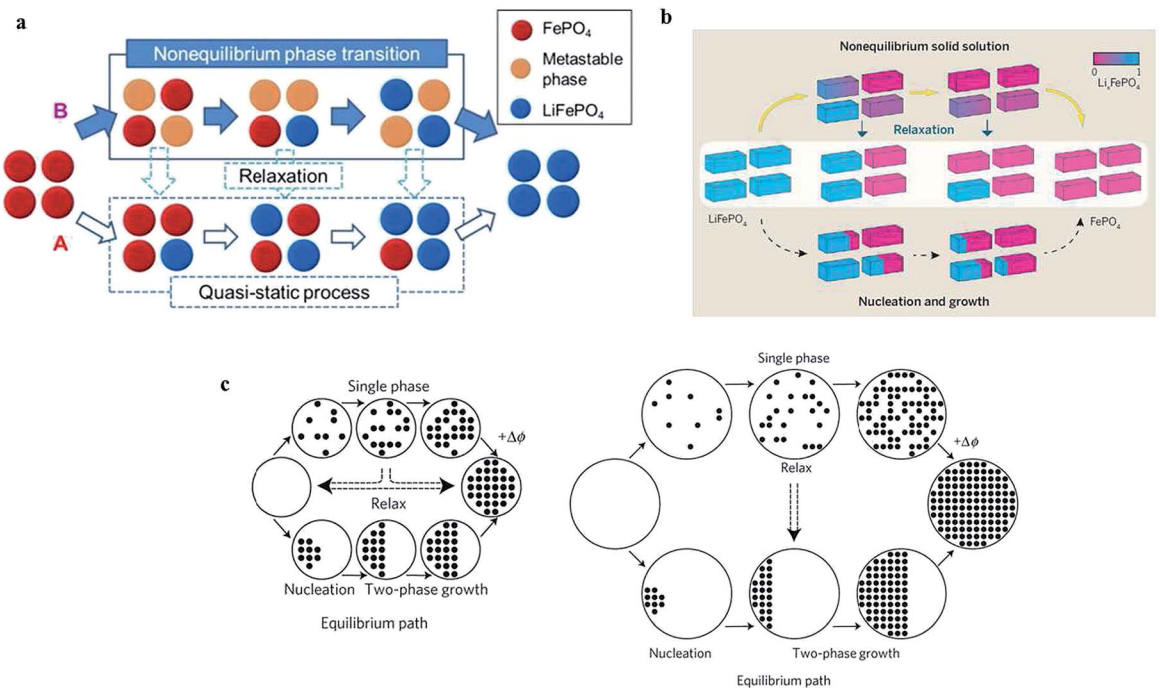

Fig. 13 Non-equilibrium phase transition *via* a metastable phase (a), solid-solution (b) and single phase model (c). Reproduced with permission from ref. 179, 180 and 19. Copyright 2013 American Chemical Society, 2014 the American Association for the Advancement of Science and 2011 Nature Publishing Group, respectively.

Table 2 Solid-solution mechanism confirmed by a variety of experimental studies

Sample	Characterization tools	Experimental method	Driven force	Ref.
500 nm particles	XRD	Chemical delithiation with NO_2BF_4	Temperature driven solid solution, Li_xFePO_4 ($0 \leq x \leq 1$)at 450 °C	165
NA	NA	Phase-field model	Current density	20
100 nm nanoparticle	NA	Density functional theory calculations	Low overpotential at non equilibrium path	19
Micrometric particle	Time-resolved XRD	Electrochemical (de)lithiation	High (de)charge rates (10 C), a metastable $Li_{0.6-0.75}FePO_4$ solid-solution phase	179
100 nm $LiMn_{0.4}Fe_{0.6}PO_4$ particles	*In operando* synchrotron XRD	Electrochemical (de)lithiation	Olivine composition, the metastable solid solution covering a remarkable wide compositional range	183
10–180 nm nanoparticles	*In situ* synchrotron XRD	Electrochemical (de)lithiation	High cycling rates, the solid solution phase, Li_xFePO_4($0 < x < 1$) covering the entire phase composition	180

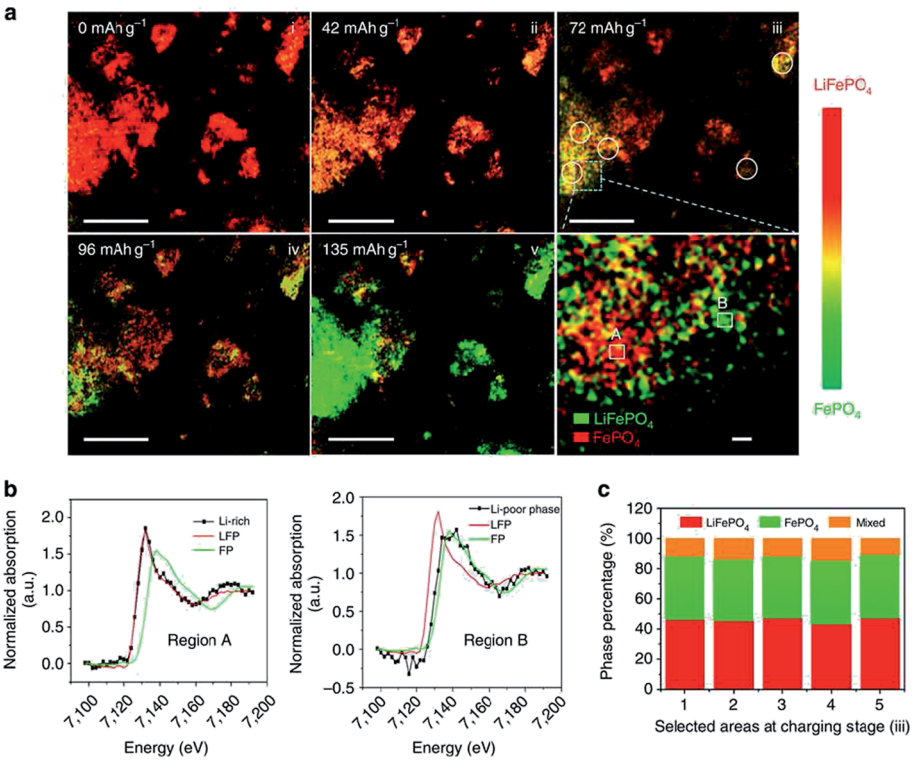

Fig. 14 *In operando* chemical mapping of a multi-particle $LiFePO_4$ system at a rate of 5 C. (a) 2D chemical mapping; (b) XANES at selected regions A and B at charging stage (iii); (c) Statistical histograms of phase compositions at five selected regions at charging stage (iii). Scale bar: 10 μm for the five 2D maps, 200 nm for the enlarged map. Reproduced with permission from ref. 159. Copyright 2014 Nature Publishing Group.

in situ soft X-ray spectroscopy also indicates that the phase transformation starts from the region adjacent to the current collectors in a $LiFePO_4$ electrode,[191] confirming the inhomogeneity in the $LiFePO_4$ phase transformation.

More direct evidence of the phase transformation comes from a recent *in operando* imaging study. Wang *et al.* tracked the phase transformation evolution on the electrode scale using transmission X-ray microscopy under *in operando* conditions.[159] The unique capability of this *in operando* imaging method is that it can work on a true coin cell without a specialized cell design, therefore, truly revealing the electrochemical process in the $LiFePO_4$ electrode. With this technique, it is suggested that there is a rate-dependent inhomogeneity behavior in a multi-particle $LiFePO_4$ system. At a slow charging rate, a homogeneous phase distribution is found and the entire electrode shows a similar chemical composition, whereas a fast charging rate leads to inhomogeneity and two-phase coexistence in the electrode. The inhomogeneous phase composition only takes place in a fast-charging $LiFePO_4$ electrode, which emphasizes the crucial role of electrode architecture in the (de)lithiation

Table 3 Synchrotron X-ray imaging techniques for $LiFePO_4$ studies

Methods	Energy range	Sample thickness	Spatial resolution	Pressure condition	*In situ* operation	Ref.
Hard X-ray microscopy	4k–13 keV	Up to micron scale	<30 nm	Ambient	Easy	129
Soft X-ray microscopy	200–2 keV	Up to hundreds of micron	<30 nm	Vacuum/half vacuum	Difficult	128

process in a multi-particle system, as the electrode structure (thickness, porosity, conductive carbon network, *etc.*) significantly affects the inter-particle intercalation pathway at high rates. This finding motivates more future efforts in optimizing the entire electrode structure to improve rate performance for $LiFePO_4$ (Fig. 14 and Table 3).

The understanding of these complex (de)lithiation mechanisms has heavily relied on advanced characterization tools. Recent advances in synchrotron X-ray technologies, in particular synchrotron X-ray microscopy, allow the probing of large volumes of battery materials at high spatial resolution with accurate chemical/electronic structural information. A new record of 5 nm resolution has recently been achieved by soft X-ray ptychography,[192] breaking through the limits of optics (Fig. 15), and will provide more powerful capabilities for elucidating the complex mechanism of battery materials.

4. Surface and interface chemistry

4.1. Surface chemistry-performance improvement

Surface chemistry plays an important role in determining the rate-performance of $LiFePO_4$. Since a $Li_4P_2O_7$-like fast ion-conductive phase was first suggested by Ceder to improve the rate-performance of $LiFePO_4$,[193] surface modification with some stable lithium-ion conductors is considered to be one of the strategies to improve lithium-ion transport in $LiFePO_4$. For example, by coating novel coralline glassy lithium phosphate onto nano-$LiFePO_4$ particles, it enhances the reversible capacity, cycle performance and rate performance. This highly effective lithium-ion conductor increases lithium-ion diffusion across the surface (010) and into the $LiFePO_4$ bulk, and improves lithium-ion transfer kinetics. In addition, this lithium-including material also provides extra lithium sources to raise the lithium capacity and improve the cycle performance of the $LiFePO_4$ electrode.[194] In addition to lithium-ion diffusion into $LiFePO_4$, the solid–electrolyte interface also plays an important role in the rate performance of LFP.[195] If the lithium diffusion kinetics at the interface can be improved, a faster charging capability may be achieved, allowing even larger sized $LiFePO_4$ (*e.g.* micron-scale) to exhibit a high rate performance. To enhance lithium diffusivity into the $LiFePO_4$ electrode, with the electrostatic attraction role, Wang *et al.* mixed $LiFePO_4$ with anion absorbents to enhance the delithiation process and the rate performance for $LiFePO_4$.[196] In spite of the enhanced electrochemical performance, the fundamental understanding of these surface ionic conductors and their true roles are still under debate, as it is always influenced by a carbon coating. Furthermore, these surface ionic conductors may not be very electron conductive and possibly may only work at some local sites, such as the (010) channel surface. The synthesis and deposition of these surface conductors at particular sites is another challenge.

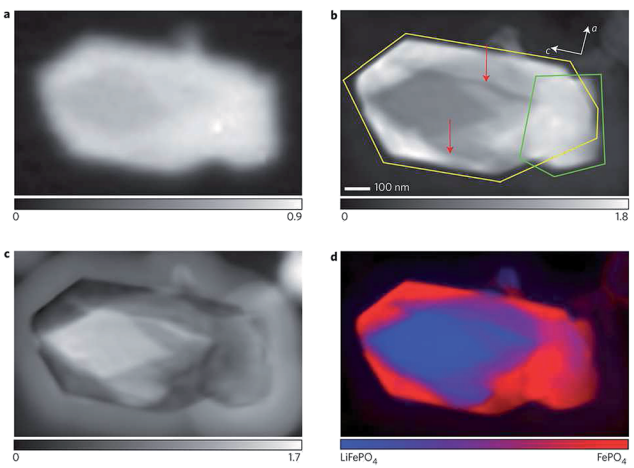

Fig. 15 X-ray microscopy of partially delithiated $LiFePO_4$. (a and b) Optical density maps from STXM (a) and ptychography (b) at 710 eV, showing the maximum. (c) Phase of the ptychographic reconstruction at 709.2 eV, showing the maximum relative phase shift between the end members. (d) Colorized composition map calculated by principal component analysis absorption contrast between the end members. Reproduced with permission from ref. 192. Copyright 2014 Nature publishing group.

4.2. Surface chemistry – new phase formation

As a simple and effective method to enhance $LiFePO_4$ conductivity, carbon coating has achieved enormous success and has been widely applied in industrial production. Nevertheless, due to the strong reducing atmosphere from carbon coating under high temperatures, the surface chemistry change of $LiFePO_4$ is unclear. With a $LiFePO_4$ ingot sample composed of a flat surface, Wang *et al.* recently found direct evidence of the significant influence of carbon coating on $LiFePO_4$ surface chemistry.[197] A size-dependent surface phase change was found in $LiFePO_4$ during carbon coating. It was found that, for large-sized $LiFePO_4$, new $Fe_2P_2O_7$ phases with poor conductivity were observed at the ingot surface, as shown in Fig. 16. This surface melting and chemistry change occurs under the reducing environment created during carbon coating, resulting in a nonstoichiometric mixture in the molten phase. During the cooling process, the new phase of $Fe_2P_2O_7$ precipitates from the nonstoichiometric molten mixture, accompanied by Li_2O loss. These surface phase changes may even occur at temperatures as low as 650 °C, which is comparable to industrial synthesis

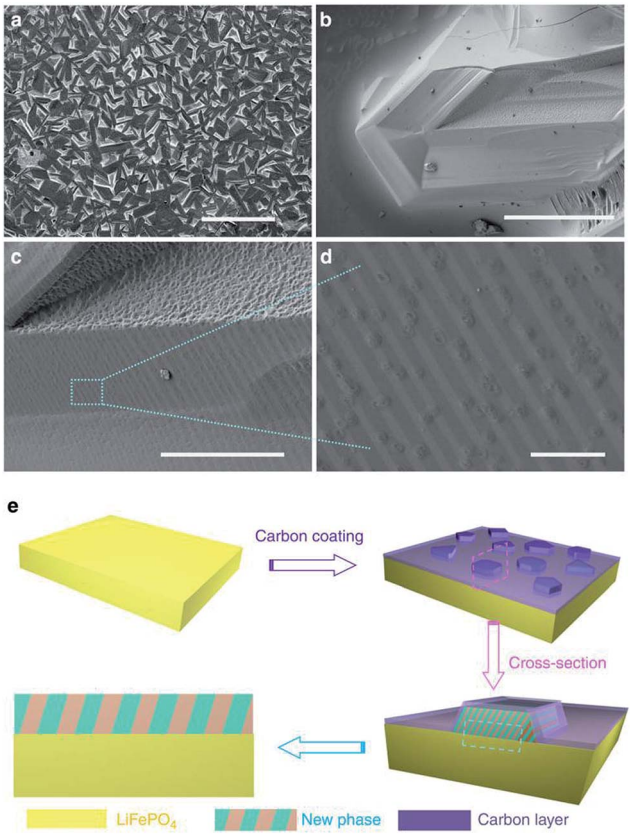

Fig. 16 (a–d) SEM image of surface phase formation on $LiFePO_4$ after carbon coating. (e) Schematic representation of surface phase formation on $LiFePO_4$. Scale bar, 1 mm (a), 500 μm (b), 100 μm (c) and 1 μm (d). Reproduced with permission from ref. 197. Copyright 2014, Nature Publishing Group.

temperature for $LiFePO_4$. In contrast, nanosized $LiFePO_4$ shows an extremely high stability. Even with carbon coating at temperatures as high as 1000 °C, $LiFePO_4$ shows a high purity without any new phase formation. This is attributed to the precipitation rate of carbon atoms on the surface of nanosized $LiFePO_4$ being higher than its diffusion rate. This leads to the rapid formation of a carbon protection layer and, accordingly, limits the further interaction between the hydrocarbons and $LiFePO_4$. Therefore, considering the industrial production of large-sized $LiFePO_4$ to improve tap density and volumetric energy density, one has to consider the possible unexpected surface phase change and the new phase formation carbon coating.

4.3. Surface chemistry-aging and storage properties

In addition to performance improvements and surface phase changes under carbon coating, most studies make a correlation between the surface chemistry and $LiFePO_4$'s aging and storage stability.[198–200] As a stable cathode material, previous studies confirm the excellent stability of $LiFePO_4$ in many conventional electrolytes upon electrochemical cycling.[201–203] In addition to the unique structure that restrains oxygen release, first principle calculations show a lower surface energy and redox potential (2.95 V) at the (010) facets than other facets. This also provides another explanation for the high stability of $LiFePO_4$ during electrochemical cycling.[95] However, in practical storage and long-term electrochemical cycling, a performance fade is still observed; especially at elevated temperatures.[204] The widely accepted reason for this is HF formation in moisture-contaminated electrolytes resulting from chemisorbed water and the presence of hydrogen bonds.[205] However, in practical applications of lithium-ion batteries, it is hard to completely avoid a very small amount of moisture; in particular, contamination may occur during cell assembly. When the $LiFePO_4$ surface is in contact with electrolytes that have a small amount of OH groups, corrosive HF is formed from the chemical reaction with nearby PF6 anions in the electrolyte.[206] As a result, iron dissolution occurs and the $LiFePO_4$'s performance decreases.

Considering iron dissolution and related material stability, the aging of $LiFePO_4$ has attracted more and more attention in studies.[207,208] An in-depth structural investigation has indicated that when moisture (water) or hydroxyl groups contaminate the electrolytes, iron(II) is oxidized to iron(III) at the surface of $LiFePO_4$ particles, possibly resulting in the formation of electrochemically inactive $LiFePO_4(OH)$ tavorite.[209] The presence of this ferric phase changes the pristine chemical composition and decreases the specific capacity of the $LiFePO_4$. It also affects the cycling and reversible electrochemical behavior, due to the inactive ferric surface layer. Furthermore, the transition metal can move to the negative electrode and be reduced to metallic clusters, resulting in the formation of solid electrolyte interphase, capacity loss and serious safety issues.[210]

Wang *et al.* recently presented a direct experimental observation of the surface aging process and iron dissolution in olivine $LiFePO_4$ that was stored in moisture-contaminated electrolyte.[211] Using a $LiFePO_4$ ingot sample with a flat surface as the model material, iron dissolution and surface chemistry changes could be clearly observed. As expected, the iron dissolution is directly related to the $LiFePO_4$ aging process. In addition to the surface chemistry of the $LiFePO_4$ material itself, the study also indicated the direct relationship between the surface aging process and the inhomogeneous surface chemistry (impurity phases). It is well known that some common impurity phases (*e.g.* Fe_2O_3, Fe_2P, Li_3PO_4, *etc.*) often exist from the $LiFePO_4$ synthesis process.[212,213] As inactive materials, the presence of these impurity phases not only decreases the utilization of active $LiFePO_4$, it also significantly affects the physical, chemical and electrochemical performance of $LiFePO_4$. It was also found that impurities may accelerate the surface aging process of $LiFePO_4$, because an oxidation–reduction reaction occurs at local sites with impurity phases, similar to the metal corrosion mechanism.[214] Iron-rich impurity phases significantly corrode, due to the lower corrosion potentials, which inhibits the corrosion of the adjacent $LiFePO_4$ bulk. In contrast, phosphorus-rich impurity phases are more stable, due to their higher corrosion potential; however, these results in the corrosion reaction occurring in the adjacent bulk $LiFePO_4$.[215]

Having elucidated where $LiFePO_4$'s failure originates, strategies to limit surface aging are suggested. The most economic and effective method to protect $LiFePO_4$'s surface is a carbon-coating layer. Recent research has shown a significant

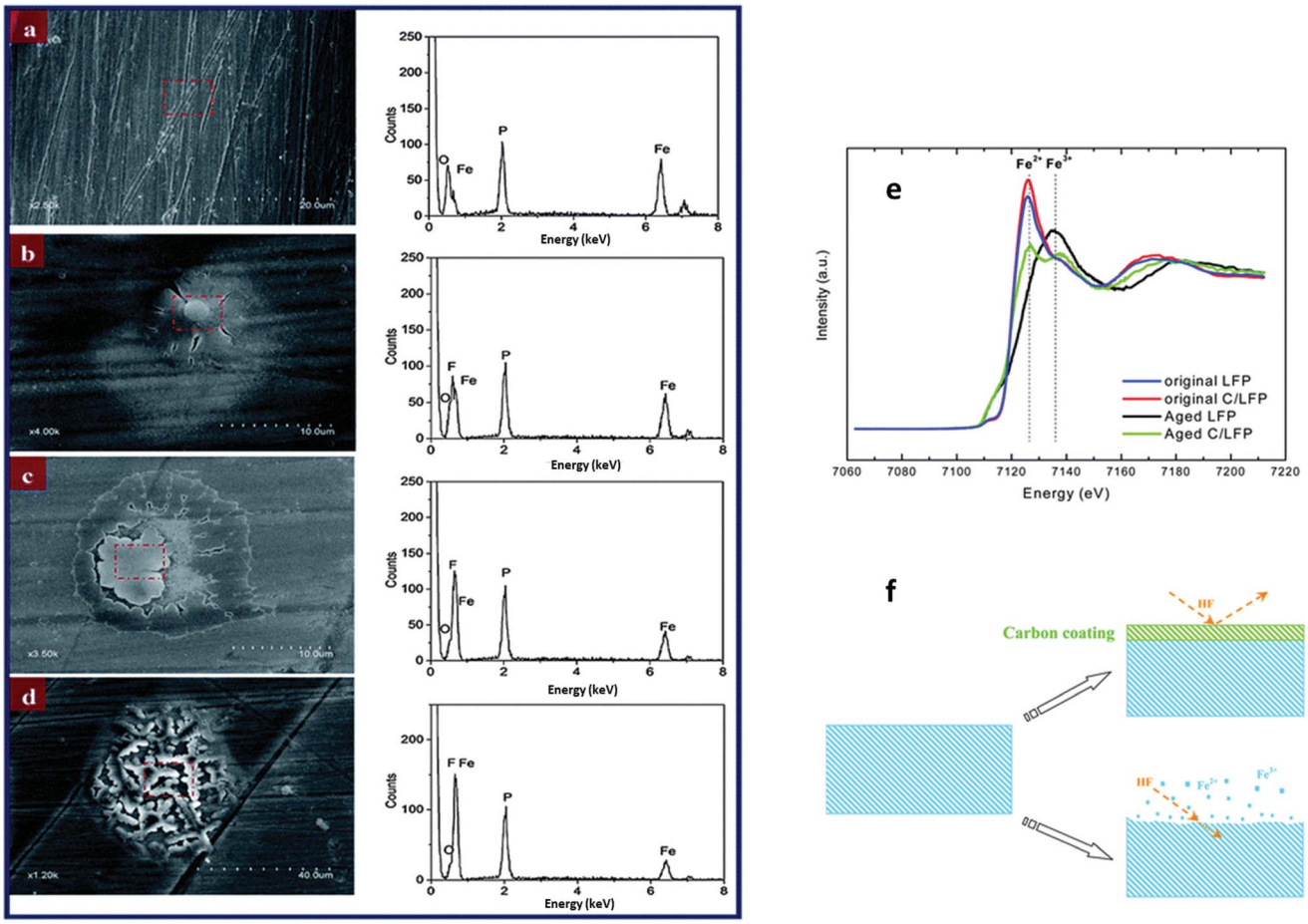

Fig. 17 (a–d) Iron element dissolving on the $LiFePO_4$ surface during the surface aging process at (a) 0 h, (b) 8 h, (c) 24 h and (d) 32 h. (e) Fe K-edge XANES spectra of pristine $LiFePO_4$ and aged $LiFePO_4$ samples. (f) Schematic illustration showing carbon layer protection for surface aging. Reproduced with permission from ref. 211. Copyright 2013, the Royal Society of Chemistry.

improvement in $LiFePO_4$ surface chemistry stability with a nano-carbon coating, as the carbon surface layer protects $LiFePO_4$ from direct contact with the corrosive medium, effectively restraining the surface corrosion and preserving the initial surface chemistry of $LiFePO_4$, as shown in Fig. 17.[211] This conclusion is clearly confirmed by the Fe K-edge XANES change found during the aging process. After the same surface aging treatment, a clear edge shift in the spectra can be observed on the bare $LiFePO_4$ without carbon coating, due to the oxidation of Fe(II) to Fe(III). In contrast, the iron valence state change is absent in the carbon-coated sample, indicating the protection role of the carbon coating for $LiFePO_4$'s surface chemistry stability.[211] In spite of the positive protection role of the carbon coating, further surface engineering to improve $LiFePO_4$ stability is still needed because a sole carbon nanolayer may not withstand the long-term electrochemical cycling. Because of the lattice parameter mismatch, there is a coherency strain between the two phases of $LiFePO_4$ and $FePO_4$. As a result, with electrochemical cycling, the stress in the electrode continuously increases, which may lead to the separation of the carbon/$LiFePO_4$ interface.[216] This separation or partial "isolation" of carbon from $LiFePO_4$ will cause the direct exposure of $LiFePO_4$ to the electrolyte, which weakens the carbon layer's protection and surface chemistry stability. In addition, the "uncovered" $LiFePO_4$ also exhibits poorer electronic conductivity. It is well known that in the case of an electrochemical reaction, both electronic and ion accessible sites are simultaneously electrochemically active. Therefore, the separation of carbon from the $LiFePO_4$ surface will decrease the number of electrochemical triple contact sites, which results in a decrease in the specific capacity and cycle performance. Therefore, further enhancement of the bonding between the carbon layer and $LiFePO_4$ is crucial for $LiFePO_4$ surface chemistry stability.

5. Olivine phosphates for sodium-ion batteries

For the demands of low-price and availability, the development of rechargeable batteries for large-scale energy systems using abundant resources and cheap raw materials has become inevitable. Sodium has many similar chemical properties to lithium, and, furthermore, is abundant, inexpensive and environmentally friendly. Thus, sodium-ion batteries are considered to be suitable alternatives to lithium-ion batteries in future

large-scale energy storage systems.[217–219] Inspired by the successful commercialization and remarkable electrochemical properties of $LiFePO_4$, the electrochemical and structural study of olivine $NaFePO_4$ has attracted much interest.[220–222] Unfortunately, current olivine $NaFePO_4$ exhibits unsatisfactory electrochemical performance in sodium-ion batteries and faces many challenges.

5.1. Asymmetry electrochemical behavior and phase transformation

One challenge is related to understanding the complex phase transformation mechanism. Although sharing the same phase structure as olivine $LiFePO_4$, $NaFePO_4$ exhibits a significantly different mechanism in both thermodynamics and reaction kinetics during Na-ion insertion/extraction. The phase transformation process occurring in Na_xFePO_4 does not proceed with a constant composition, therefore, the results and conclusions for lithium-ion batteries may not be directly applied or transferable to sodium-ion batteries.[223]

Different from the one charge/discharge plateaus for $LiFePO_4$, the charge/discharge profile and CV show two plateaus (~2.88 V and ~3.02 V *vs.* Na/Na^+) for $NaFePO_4$ when charging, but only one plateau when discharging.[224–226] It seems that the two potential plateaus are separated by the formation of an intermediate phase (Na ~ $0.7FePO_4$) during the desodiation process (from $NaFePO_4$ to $FePO_4$), but the three phases ($FePO_4$, $NaFePO_4$, Na ~ $0.7FePO_4$) appear simultaneously during the sodiation process (from $FePO_4$ to $NaFePO_4$). This asymmetry in electrochemical behavior may be related to the larger structural mismatch, in which a 17.58% volume difference is found with $FePO_4/NaFePO_4$, two times higher than $FePO_4/LiFePO_4$.[227] Furthermore, the redox potential gap in $NaFePO_4$ is much larger (3–4 times) than the one in $LiFePO_4$, which also explains the poorer Na ion insertion/extraction kinetics in $NaFePO_4$, in comparison to $LiFePO_4$ (Fig. 18).

More and more experimental results and structural analysis confirm the two-step desodiation process in $NaFePO_4$. During the first step, sodium is extracted from $NaFePO_4$ through a single homogeneous phase process up to the intermediate phase, when $Na_{2/3}FePO_4$ forms at the voltage discontinuity (that is, a solid solution process for Na_xFePO_4, $1 > x > 2/3$). In the second step, sodium extraction occurs in a two-phase process between a Na-rich Na_yFePO_4 phase and a Na-poor $FePO_4$ phase whose composition has been found to vary with overall Na content in the electrode (that is, a two-phase process between $Na_{2/3}FePO_4$ and $FePO_4$). As a result, contrary to the symmetrical biphasic mechanism observed in micrometric $LiFePO_4$, Na extraction occurs in two voltage plateaus separated by an intermediate phase Na_xFePO_4 ($x \sim 2/3$), whereas three phases ($FePO_4$, $Na_{2/3}FePO_4$ and $NaFePO_4$) appear simultaneously

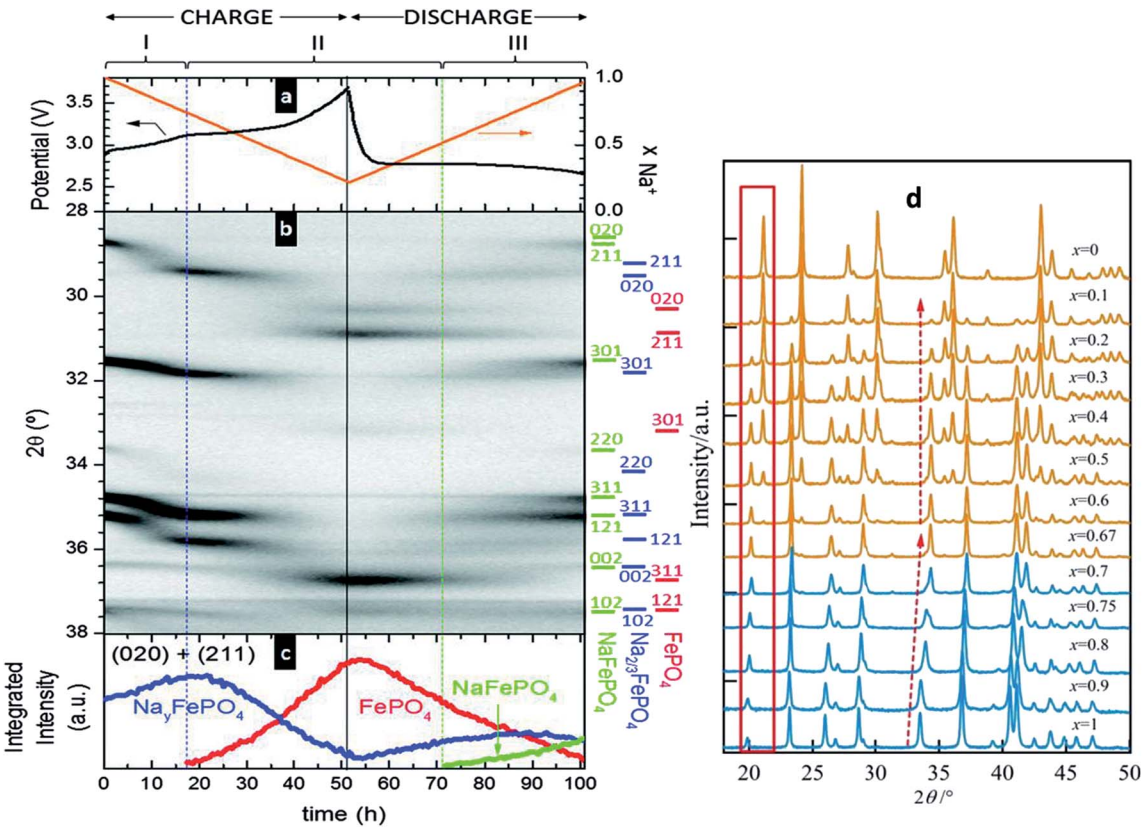

Fig. 18 (a–c) *In situ* XRD of $NaFePO_4$ under the charge/discharge cycles. (b) The detailed XRD patterns at a full cycle (charge and discharge). (c) Summary of the integrated intensity of the (020) and (211) reflections for each of the formed phases.[194] Reproduced with permission from ref. 227. Copyright 2014, the Royal Society of Chemistry. (d) XRD spectra of Na_xFePO_4 as functions of x, a single phase zone ($2/3 < x < 1$), and a mixture of $Na_{2/3}FePO_4$ and $FePO_4$ zone ($x < 2/3$). Reproduced with permission from ref. 226. Copyright 2014, the American Chemistry Society.

during Na insertion.[225] The crystal structure of $Na_{2/3}FePO_4$ has been recently studied in detail with synchrotron X-ray diffraction and defined as a superstructure due to Na/vacancies and charge ordering.[228,229] The intermediate phase at $x = 2/3$ for Na_xFePO_4 is also much more stable, compared to the lithium equivalent. The large cell mismatch enhances the effects of the diffuse interface, which has a higher impact on the Na-ion than Li-ion intercalation chemistry, and therefore a reduced miscibility gap in the overall composition are observed here in micrometric materials.[227] Recently, a detailed understanding of the intermediate phase, $Na_{2/3}FePO_4$, has been reported. With a variety of characterization methods, Boucher *et al.* proposed a three-fold superstructure for the $Na_{2/3}FePO_4$ intermediate phase, with a dense plane being formed by the 2/3 Na and 1/3 vacancy sub-lattice in the intermediate phase, related to the second/third shortest Na–Na distances.[230] This finding introduces a new strategy to develop high-rate olivine cathodes for Na-ion batteries by producing grains with larger (101) surface areas.

Due to the different phase transformation thermodynamics, the reaction kinetics (rate performance) and cycling stability of $NaFePO_4$ were also shown to be much worse than $LiFePO_4$. For example, a specific capacity of 147 mA h g^{-1} for $NaFePO_4$ was reported during the first cycle for the battery operated at 60 °C and a $C/24$ rate, but it quickly decreased to 50.6 mA h g^{-1} in the second cycle and the cyclability was limited to 4–5 cycles.[220,231] A comparative study between olivine $NaFePO_4$ and $LiFePO_4$ with identical physical properties (particle size, particle size distribution, surface coating, and active material loading, *etc.*) confirms the different thermodynamics and kinetics. The slow sodium ion kinetics in $NaFePO_4$ is considered to be due to a number of factors; (i) the Na ion's diffusion coefficient is 1–2 magnitude lower than Li, (ii) much poorer electronic conductivity, and (iii) the larger volume change in $NaFePO_4/FePO_4$ (Fig. 19).[232]

5.2. Triphylite and maricite $NaFePO_4$

Different from $LiFePO_4$, $NaFePO_4$ is composed of two different crystal structures, maricite and triphylite (Fig. 20). Maricite $NaFePO_4$ is more thermodynamically stable, but in the maricite $NaFePO_4$ framework, Na^+ and Fe^{2+} occupy the M2 and M1 sites (edge-sharing FeO_6–FeO_6 units), which is the opposite of olivine $LiFePO_4$. As a result, the connectivity of a sodium and iron octahedral in this maricite framework blocks the Na ion diffusion channels, limiting Na ion insertion and extraction. In contrast, the metastable triphylite $NaFePO_4$ has corner-sharing FeO_6 units and edge-sharing FeO_6–PO_4. As a result, similar to $LiFePO_4$'s electrochemical behavior, triphylite $NaFePO_4$ allows

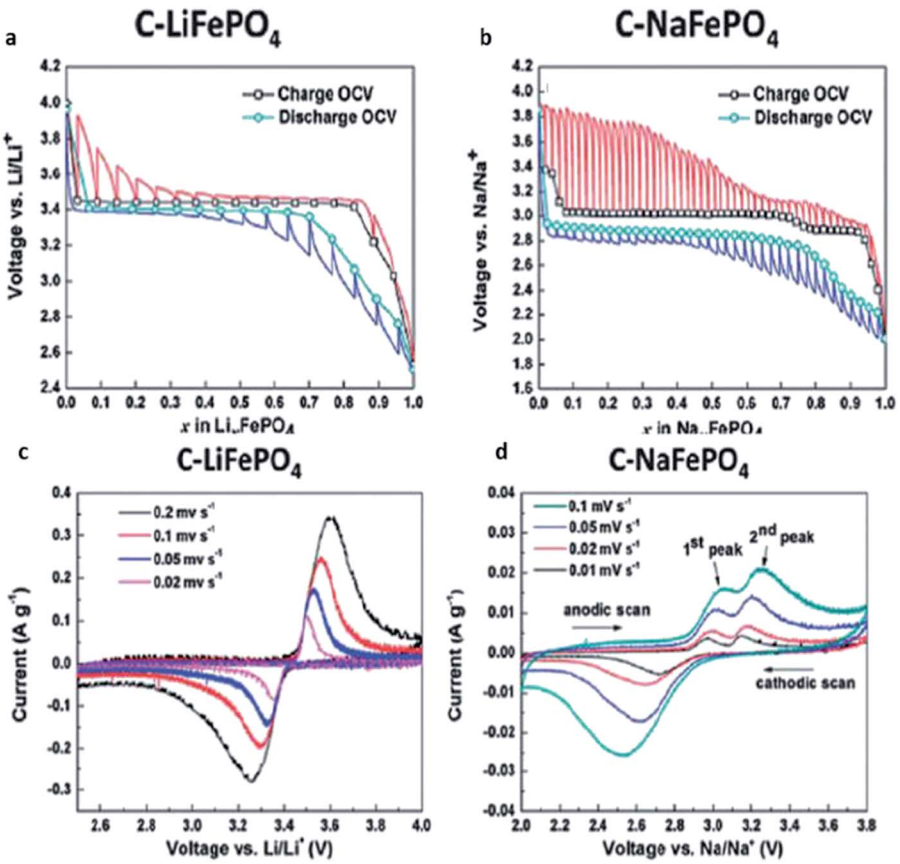

Fig. 19 (a and b) Equilibrium (open-circuit)–voltage (symbols) and transient voltage profiles (solid lines) for C-$LiFePO_4$ and C-Na_xFePO_4. (c and d) Cyclic voltammetry (CV) of C-$LiFePO_4$ in the Li-ion batteries and C-$NaFePO_4$ in the Na-ion batteries. Reproduced with permission from ref. 232. Copyright 2014, the Royal Society of Chemistry.

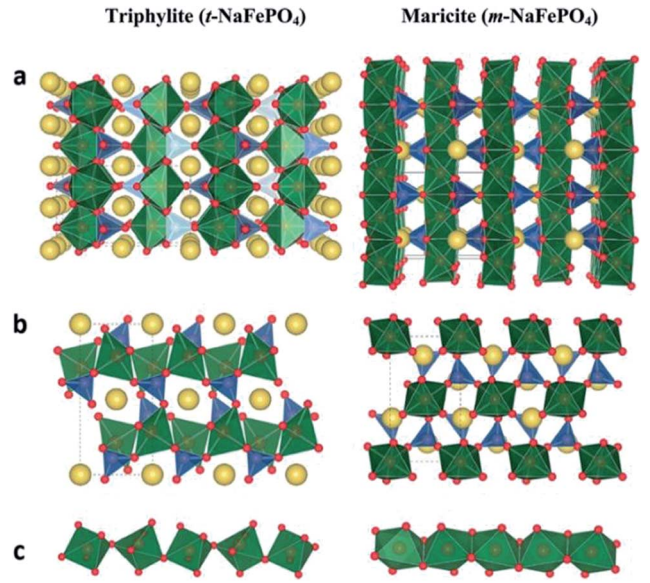

Fig. 20 (a and b) Schematic showing orthorhombic structured triphylite $NaFePO_4$ (left) and maricite $NaFePO_4$ (right). FeO_6 octahedra (green), PO_4 tetrahedra (blue), and Na atoms (yellow). (c) Corner-sharing and edge-sharing coordinations among chains of neighboring FeO_6 octahedra for the two structures. Reproduced with permission from ref. 233. Copyright 2014, American Chemical Society.

one-dimensional Na ion diffusion along the *b* direction and can deliver over 120 mA h g^{-1} in capacity for sodium-ion batteries. In addition, the electrostatic repulsion between iron and phosphorus also increases the Fe–O bond lengths, contributing to a higher redox potential of $FePO_4$/$NaFePO_4$.[233]

Although the maricite $NaFePO_4$ is theoretically electrochemically inactive, a more recent study has demonstrated that sodium ions can be extracted/inserted reversibly from maricite $NaFePO_4$ at slow rates. Nevertheless, the delivered capacity is only 1/3 of the theoretical capacity, due to the absence of the Na ion diffusion channels. It is evident that further understanding the $NaFePO_4$ structure and its correlation to electrochemical performance is needed to advance this promising material.[218]

5.3. Strategies for electrochemically active $NaFePO_4$

As discussed above, a big challenge in current $NaFePO_4$ research is the synthesis of electrochemically active $NaFePO_4$. Different from $LiFePO_4$, $NaFePO_4$ synthesized by many conventional methods, such as classic solid-state routes, exhibits poor capacity and irreversibility. This is due to the conventional synthesis methods usually producing the thermodynamically stable but electrochemically inactive maricite phase.[234,235] Currently, electrochemically active $NaFePO_4$ with an olivine phase can be mainly obtained *via* the chemical or electrochemical insertion of sodium ions into olivine $FePO_4$.[236–238] In general, this process can be performed through a two-step procedure, involving: (1) the delithiation of $LiFePO_4$ in a lithium cell, and (2) the use of the delithiated electrode ($FePO_4$) in a new cell, replacing lithium with sodium as the anode. However, for easy handling and safety concerns, it is desirable to use alternative anode materials other than sodium metal in practical applications. Similar to a lithium-ion battery, Hasa *et al.* reported a new sodium-ion battery with a $NaFePO_4$ cathode and a Sn–C sodium-alloying anode.[239] The $NaFePO_4$ cathode was obtained by Li–Na conversion of a $LiFePO_4$ cathode directly in a full cell with a sodium-ion electrolyte. The results show that this strategy enables the efficient conversion of $LiFePO_4$ to $NaFePO_4$ at a voltage of 3 V, resulting in the battery showing a superior maximum capacity of 150 mA h g^{-1}, and a high rate capability and cycle performance.

In addition to the chemical/electrochemical sodiation method, Nazar's group recently reported the topochemical synthesis of electrochemically active $Na[Mn_{1-x}M_x]PO_4$ (M = Fe, Ca, Mg), where $0 < x < 0.5$, *via* a low-temperature solid-state method.[211] In the topochemical reaction, a molten salt reaction converts $NH_4[Mn_{1-x}M_x]PO_4 \cdot H_2O$ (M = Fe, Ca, Mg) to electrochemically active $Na[Mn_{1-x}M_x]PO_4$. Furthermore, the obtained $Na(Fe_{0.5}Mn_{0.5})PO_4$ exhibits a solid-solution behavior, which is attributed to the large interface strain, due to the large Na ion size. This novel olivine material and synthesis method also opens new opportunities to further develop this olivine cathode for Na-ion batteries.

Another alternative strategy to avoid the direct synthesis of olivine $NaFePO_4$ is by using chemically easily synthesized $FePO_4$ as the cathode material for Na-ion batteries.[240–242] Due to its lower processing temperature, amorphous $FePO_4$ is easier to synthesize and exhibits an acceptable electrochemical performance. Furthermore, the isotropic and defect-free nature of amorphous $FePO_4$ provides a large amount of continuous pathways for Na ions.[243,244] Similar to pristine $LiFePO_4$, $FePO_4$'s conductivity needs to be further improved before its application in sodium-ion batteries. By using carbon nanotubes and graphene, the C/$FePO_4$ composite exhibits an enhanced electrochemical performance.[245,246] Recently, with the functionalization of rhodanine-acetic acid–pyrene, $FePO_4$ was directly grown on graphene nanosheets. The obtained $FePO_4$/graphene hybrids showed superior capacity and rate capability in sodium-ion batteries.[247] Another report involves the synthesis of $FePO_4$ nanospheres *via* a simple precipitation method. Benefiting from the mesoporous structure and superior carbon conductive network, the C/$FePO_4$ nanospheres exhibited a high initial discharge capacity (151 mA h g^{-1} at 20 mA g^{-1} rate), a high rate capability (44 mA h g^{-1} at 1000 mA g^{-1}) and a superior cycle stability (94% capacity retention ratio over 160 cycles).[248]

Layered A_2FePO_4F (A = Na, Li) was first reported by Ellis *et al.*[249] as a new cathode in either Na-ion or Li-ion batteries. With the layer structure created by interconnected Fe_4F_2–PO_4, this class of material allows 2D ion-diffusion pathways for Na^+ and Li^+, and exhibits a small volume change (3.7%), with negligible stress.[216] The superior structural stability and 2D ion-diffusion makes this class of material promising as the cathode material for both Li-ion and Na-ion batteries.[250] Furthermore, in contrast to $NaFePO_4$, Na_2FePO_4F can be easily synthesized and is electrochemically active. For example, with a common solid-state method, the synthesized $NaFePO_4$ is inactive, but Na_2FePO_4F exhibits a discharge capacity of 116 mA h g^{-1} at 0.1 C with good cycle stability.[251] Therefore, the synthesis of

Na_2FePO_4F is another possible solution to maricite $NaFePO_4$. In spite of these advantages, the poor electronic conductivity poses big challenges for the practical application of Na_2FePO_4F in sodium-ion batteries. To overcome this challenge, similar to $LiFePO_4$, carbon coating, size reduction and nanostructure design strategies are widely applied for the synthesis of high performance Na_2FePO_4F.[252,253]

6. Concluding remarks and future directions

To meet the strict demands of large-scale energy storage systems, such as in electric vehicles, lithium-ion batteries must achieve high safety, long lifetime, low cost, high specific capacity, high rate performance and volumetric energy density. Although $LiFePO_4$ is advantageous in terms of safety, lifetime, cost and specific capacity, the fast charging/discharging property and high volumetric energy density pose critical challenges. Size reduction to the nanoscale is a common strategy to improve rate performance, but it also directly leads to a poor volumetric energy density. This is particularly important for $LiFePO_4$, since the theoretical density (3.68 g cm^{-3}) of $LiFePO_4$ is much lower than many other cathodes (*e.g.* 5.1 g cm^{-3} for $LiCoO_2$, 4.8 g cm^{-3} for $LiNiO_2$ and 4.2 g cm^{-3} for $LiMn_2O_4$). As a result, the exploration of novel methods, not solely relying on the nano route, is urgently needed to significantly enhance the rate performance, while keeping the tap density at an acceptable value (such as above 1.5 g cm^{-3}). The essential breakthrough in finding a high rate performance needs an understanding of the underlying kinetics in phase transformation mechanism that is responsible for fast charge/discharge. Recent advances in *in situ* characterization methods provide direct experimental evidence of the solid-solution and intermediate-phase mechanisms during the $LiFePO_4$ phase transformation process under normal operating conditions. This is not the case when using extremely high temperatures (350 °C) or small particle sizes (smaller than 40 nm), which drives the design of novel olivine lithium metal phosphate materials with possible solid-solution phase transformation *via* surface and/or structural modification. This is confirmed by recent findings of the extended solid solution and coherent transformation in $LiMn_{0.4}Fe_{0.6}PO_4$ *via in situ* synchrotron XRD, which explains the rate capability exceeding that of $LiFePO_4$.[189] In addition, to meet the high volumetric energy density, the development of new synthesis routes to produce micron-scale $LiFePO_4$ secondary structures, while maintaining its rate performance, are still expected. Current secondary-particle technology allows the tight packing of primary nanoparticles to increase tap densities, but further development is still needed.

Understanding the surface chemistry and interface between carbon and $LiFePO_4$ also plays a critical role in lithium intercalation kinetics and material stability. Some surface phase formation is dependent upon the carbon-coating process (size-dependent) and storage circumstance (moisture). In addition, practical manufacturing processes of $LiFePO_4$ may be accompanied by the formation of different impurities, such as the iron and phosphorus phases, depending on the preparation conditions. These impurities may block the 1D lithium-ion diffusion channels, hindering the effective (de)lithiation capability and reducing the capacity. The existence of these small amounts of impurities also may "poison" $LiFePO_4$, as it can degrade the surface chemistry stability, storage stability and aging process. In addition, the material's homogeneity and production costs are important factors in its large-scale application for EVs. The development of an inexpensive synthesis process by simplifying the processing steps/time, reducing the energy consumption and selecting cheap raw materials accelerates the feasibility of $LiFePO_4$ for use in large-scale applications. The newly developed molten state method provides an economic and effective route to achieve these goals.[165,213,254]

Another future research trend is the extension of $LiFePO_4$ to another olivine family, mainly $LiMnPO_4$, due to its high operating voltage (4.1 V *vs.* Li^+/Li) and accessible electrolyte voltage windows. However, the poorer electron and the ion conductivity and the Jahn–Teller distortion in $LiMnPO_4$ leads to a limited capacity, making it currently uncompetitive with $LiFePO_4$. In addition, compared to the widely studied $LiFePO_4$, the understanding of the phase transformation mechanism, the structural change upon cycling and the thermal stability of $LiMnPO_4$ is still in its infancy. Some inconsistency has been reported for these two olivine lithium phosphates, therefore, they deserve more comprehensive studies. Furthermore, carbon coating seems to be more difficult for $LiMnPO_4$, due to the poor catalytic effect of Mn. One strategy is to apply core/shell structure $LiMnPO_4/LiFePO_4$, which takes full advantage of the better carbon coating on $LiFePO_4$.[255–258] In particular, some new coating techniques, such as atomic layer deposition for thin and uniform $LiFePO_4$, should be considered.[105] Considering these difficulties, an alternative solution is the development of $LiFe_yMn_{1-y}PO_4$ materials, which combine the advantages of iron (easy carbon coating, high accessible capacity and safety) and Mn (high voltage). The presence of a solid-solution composition also allows a fast charge/discharge rate for this binary olivine lithium phosphate.

Benefiting from the success of lithium-ion batteries, recent research in olivine phosphates has been extended to its sodium analogue, $NaFePO_4$, a cathode material for Na-ion batteries. Nevertheless, the presence of two distinct structures (triphylite and maricite) make it difficult to obtain the desired battery material, as the thermodynamically stable maricite is electrochemically inactive. Current active $NaFePO_4$ are mainly synthesized by an electrochemical sodiation method, which is not suitable for future large-scale production. Therefore, a simple and feasible chemical method to directly synthesize electrochemically active $NaFePO_4$ is highly needed, but is very challenging. With regard to these challenges, at this stage, two solutions have been tested. One is the development of amorphous $FePO_4$ with good electrochemical performance, which can be prepared *via* a direct chemical synthesis route, and the other is the use of a binary metal olivine phosphate, such as $Na(Fe_{0.5}Mn_{0.5})PO_4$, that could be obtained directly by a molten salt reaction.[222] Overall, although $NaFePO_4$ is similar to $LiFePO_4$

in some important respects, it still has a long way to go to see practical application in the energy storage market.

Acknowledgements

This work was supported by Nature Sciences and Engineering Research Council of Canada (NSERC), Canada Research Chair (CRC) Program, Canada Foundation for Innovation (CFI), Ontario Research Fund (ORF), the Canada Light Source (CLS) at University of Saskatchewan, the Canadian Centre for Electron Microscopy (CCEM) at McMaster University, and University of Western Ontario. We gratefully acknowledge Craig Langford and Kaixi Wang for their help in the discussion and English polishing for this paper.

Notes and references

1 A. K. Padhi, K. S. Nanjundaswamy and J. B. Goodenough, *J. Electrochem. Soc.*, 1997, **144**, 1188–1194.
2 Y. Wang, P. He and H. Zhou, *Energy Environ. Sci.*, 2011, **4**, 805–817.
3 D. Li and H. Zhou, *Mater. Today*, 2014, **17**, 451–463.
4 J. B. Goodenough and K. S. Park, *J. Am. Chem. Soc.*, 2013, **135**, 1167–1176.
5 L. X. Yuan, Z. H. Wang, W. X. Zhang, X. L. Hu, J. T. Chen, Y. H. Huang and J. B. Goodenough, *Energy Environ. Sci.*, 2011, **4**, 269–284.
6 C. Delacourt, P. Poizot, S. Levasseur and C. Masquelier, *Electrochem. Solid-State Lett.*, 2006, **9**, A352–A355.
7 H. Huang, S. C. Yin and L. F. Nazar, *Electrochem. Solid-State Lett.*, 2001, **4**, A170–A172.
8 N. Ravet, Y. Chouinard, J. F. Magnan, S. Besner, M. Gauthier and M. Armand, *J. Power Sources*, 2001, **97–98**, 503–507.
9 K. Zaghib, M. Dontigny, A. Guerfi, P. Charest, I. Rodrigues, A. Mauger and C. M. Julien, *J. Power Sources*, 2011, **196**(8), 3949–3954.
10 L. Laffont, C. Delacourt, P. Gibot, M. Yue Wu, P. Kooyman, C. Masquelier and J. Marie Tarascon, *Chem. Mater.*, 2006, **18**, 5520–5529.
11 D. Morgan, A. Van der Ven and G. Ceder, *Electrochem. Solid-State Lett.*, 2004, **7**, A30–A32.
12 Y. Wu, Z. Wen and J. Li, *Adv. Mater.*, 2011, **23**, 1126–1129.
13 M. S. Islam, D. J. Driscoll, C. A. J. Fisher and P. R. Slater, *Chem. Mater.*, 2005, **17**, 5085–5092.
14 X. J. Wang, H. Y. Chen, X. Yu, L. Wu, K. W. Nam, J. Bai, H. Li, X. Huang and X.-Q. Yang, *Chem. Commun.*, 2011, **47**, 7170–7172.
15 X. Yu, Q. Wang, Y. Zhou, H. Li, X. Q. Yang, K. W. Nam, S. N. Ehrlich, S. Khalid and Y. S. Meng, *Chem. Commun.*, 2012, **48**, 11537–11539.
16 N. Sharma, V. K. Peterson, M. M. Elcombe, M. Avdeev, A. J. Studer, N. Blagojevic, R. Yusoff and N. Kamarulzaman, *J. Power Sources*, 2010, **195**, 8258–8266.
17 Y. Orikasaa, T. Maeda, Y. Koyama, T. Minato, H. Murayama, K. Fukuda, H. Tanida, H. Arai, E. Matsubara, Y. Uchimoto and Z. Ogumi, *J. Electrochem. Soc.*, 2013, **160**, 3061–3065.
18 C. M. Wang, W. Xu, J. Liu, D. W. Choi, B. Arey, L. V. Saraf, J. G. Zhang, Z. G. Yang, S. Thevuthasan, D. R. Baer and N. Salmon, *J. Mater. Res.*, 2011, **25**, 1541–1547.
19 R. Malik, F. Zhou and G. Ceder, *Nat. Mater.*, 2011, **10**, 587–590.
20 P. Bai, D. A. Cogswell and M. Z. Bazant, *Nano Lett.*, 2011, **11**, 4890–4896.
21 N. Sharma, X. Guo, G. Du, Z. Guo, J. Wang, Z. Wang and V. K. Peterson, *J. Am. Chem. Soc.*, 2012, **134**, 7867–7873.
22 M. Wagemaker, D. P. Singh, W. J. H. Borghols, U. Lafont, L. Haverkate, V. K. Peterson and F. M. Mulder, *J. Am. Chem. Soc.*, 2011, **133**, 10222–10228.
23 M. Safari and C. Delacourt, *J. Electrochem. Soc.*, 2011, **158**, 1123–1135.
24 Y. Zhang, C. Y. Wang and X. Tang, *J. Power Sources*, 2011, **196**, 1513–1520.
25 C. M. Julien, A. Mauger and K. Zaghib, *J. Mater. Chem.*, 2011, **21**, 9955–9968.
26 L. Castro, R. Dedryvère, J.-B. Ledeuil, J. Bréger, C. Tessier and D. Gonbeau, *J. Electrochem. Soc.*, 2012, **159**, 357–363.
27 V. Palomares, P. Serras, I. Villaluenga, K. B. Hueso, J. Carretero-González and T. Rojo, *Energy Environ. Sci.*, 2012, **5**, 5884–5901.
28 S. P. Ong, V. L. Chevrier, G. Hautier, A. Jain, C. Moore, S. Kim, X. Ma and G. Ceder, *Energy Environ. Sci.*, 2011, **4**, 3680–3688.
29 M. Casas-Cabanas, V. V. Roddatis, D. Saurel, P. Kubiak, J. Carretero-González, V. Palomares, P. Serras and T. Rojoa, *J. Mater. Chem.*, 2012, **22**, 17421–17423.
30 P. Moreau, D. Guyomard, J. Gaubicher and F. Boucher, *Chem. Mater.*, 2010, **22**(14), 4126–4128.
31 J. Wang and X. Sun, *Energy Environ. Sci.*, 2012, **5**, 5163–5185.
32 J. D. Wilcox, M. M. Doeff, M. Marcinek and R. Kostecki, *J. Electrochem. Soc.*, 2007, **154**, 389–395.
33 J. D. Wilcox, M. M. Doeff, M. Marcinek and R. Kostecki, *Solid State Ionics*, 2008, **179**, 1810–1815.
34 Y. Wang, R. Mei and X. Yang, *Ceram. Int.*, 2014, **40**, 8439–8444.
35 Z. X. Chi, W. Zhang, F.-Q. Cheng, J.-T. Chen, A.-M. Cao and L.-J. Wan, *RSC Adv.*, 2014, **4**, 7795–7798.
36 J. Chen, Y.-C. Zou, F. Zhang, Y. C. Zhang, F.-F. Guo and G.-D. Li, *J. Alloys Compd.*, 2013, **563**, 264–268.
37 A. Ponrouch, A. R. Goñi, M. T. Sougrati, M. Ati, J.-M. Tarascon, J. Nava-Avendañoad and M. R. Palacín, *Energy Environ. Sci.*, 2013, **6**, 3363–3371.
38 S. Yoon, C. Liao, X. G. Sun, C. A. Bridges, R. R. Unocic, J. Nanda, S. Dai and M. P. Paranthaman, *J. Mater. Chem.*, 2012, **22**, 4611–4614.
39 J. Yang, J. Wang, X. Li, D. Wang, J. Liu, G. Liang, M. Gauthier, Y. Li, D. Geng, R. Li and X. Sun, *J. Mater. Chem.*, 2012, **22**, 7537–7543.
40 X. L. Yang, G. Peng, L. L. Zhang, G. Liang, S. Duan, Y. H. Huang, A. Lgnatov and M. C. Croft, *J. Electrochem. Soc.*, 2012, **159**(12), A2096–A2099.
41 Y. Jin, C. P. Yang, X. H. Rui, T. Cheng and C. H. Chen, *J. Power Sources*, 2011, **196**, 5623–5630.

42 Y. Qu, J. Cao, R. Guo and W. Xu, *Electrochem. Solid-State Lett.*, 2012, **15**(2), A15–A18.
43 Z. Ma, G. Shao, X. Qin, Y. Fan, G. Wang, J. Song and T. Liu, *J. Power Sources*, 2014, **269**, 194–202.
44 S. X. Zhao, H. Ding, Y. C. Wang, B. H. Li and C. W. Nan, *J. Alloys Compd.*, 2013, **566**, 206–211.
45 F. Cheng, S. Wang, A.-H. Lu and W. C. Li, *J. Power Sources*, 2013, **229**, 249–257.
46 H. D. Asfaw, M. R. Roberts, C. W. Tai, R. Younesi, M. Valvo, L. Nyholm and K. Edström, *Nanoscale*, 2014, **6**, 8804–8813.
47 H. Ni, J. Liu and L. Z. Fan, *Nanoscale*, 2013, **5**, 2164–2168.
48 J. Zhao, J. He, J. Zhou, Y. Guo, T. Wang, S. Wu, X. Ding, R. Huang and H. Xue, *J. Phys. Chem. C*, 2011, **115**, 2888–2894.
49 C. Sun, S. Rajasekhara, J. B. Goodenough and F. Zhou, *J. Am. Chem. Soc.*, 2011, **133**, 2132–2135.
50 J. Zhou, H. Liu and Z. P. Li, *Solid State Ionics*, 2013, **244**, 23–29.
51 Y. Shi, S. L. Chou, J. Z. Wang, D. Wexler, H. J. Li, H. K. Liu and Y. Wu, *J. Mater. Chem.*, 2012, **22**, 16465–16470.
52 X. Zhou, F. Wang, Y. Zhu and Z. Liu, *J. Mater. Chem.*, 2011, **21**, 3353–3358.
53 W. T. Geng, D. H. Ping, J. Nara and T. Ohno, *J. Phys. Chem. C*, 2012, **116**, 17650–17656.
54 C. Su, X. Bu, L. Xu, J. Liu and C. Zhang, *Electrochim. Acta*, 2012, **64**, 190–195.
55 Y. Zhang, W. Wang, P. Li, Y. Fu and X. Ma, *J. Power Sources*, 2012, **210**, 47–53.
56 W. Wei, W. Lv, M. B. Wu, F. Y. Su, Y. B. He, B. Li, F. Kang and Q. H. Yang, *Carbon*, 2013, **57**, 530–533.
57 D. Zhao, Y. L. Feng, Y. G. Wang and Y. Y. Xia, *Electrochim. Acta*, 2013, **88**, 632–638.
58 L. Hu, F. Wu, C. Lin, A. N. Khlobystov and L. Li, *Nat. Commun.*, 2013, **4**, 1687.
59 Y. Liang, D. Wu, X. Feng and K. Müllen, *Adv. Mater.*, 2009, **21**, 1679–1683.
60 C. E. Hamilton, J. R. Lomeda, Z. Sun, J. M. Tour and A. R. Barron, *Nano Lett.*, 2009, **9**(10), 3460–3462.
61 J. Yang, J. Wang, Y. Tang, D. Wang, X. Li, Y. Hu, R. Li, G. Liang, T.-K. Sham and X. Sun, *Energy Environ. Sci.*, 2013, **6**, 1521–1528.
62 H. R. Byon, B. M. Gallant, S. W. Lee and Y. Shao-Horn, *Adv. Funct. Mater.*, 2013, **23**, 1037–1045.
63 Y. Li, Y. Zhao, H. Cheng, Y. Hu, G. Shi, L. Dai and L. Qu, *J. Am. Chem. Soc.*, 2012, **134**, 15–18.
64 W. Chen, L. Yan and P. R. Bangal, *Carbon*, 2010, **48**, 1146–1152.
65 Q. B. Zheng, M. M. Gudarzi, S. J. Wang, Y. Geng, Z. Li and J.-K. Kim, *Carbon*, 2011, **49**, 2905–2916.
66 Z. Wang, D. Xu, Y. Huang, Z. Wu, L. Wang and X. Zhang, *Chem. Commun.*, 2012, **48**, 976–978.
67 Q. Fan, L. Lei, X. Xu, G. Yin and Y. Sun, *J. Power Sources*, 2014, **257**, 65–69.
68 Y. Zhang, W. Wang, P. Li, Y. Fu and X. Ma, *J. Power Sources*, 2012, **210**, 47–53.
69 S. W. Oh, Z. D. Huang, B. Zhang, Y. Yu, Y. B. He and J. K. Kim, *J. Mater. Chem.*, 2012, **22**, 17215–17221.
70 Y. Ding, Y. Jiang, F. Xu, J. Yin, H. Ren, Q. Zhuo, Z. Long and P. Zhang, *Electrochem. Commun.*, 2010, **12**, 10–13.
71 T. Lin, J. Chen, H. Bi, D. Wan, F. Huang, X. Xie and M. Jiang, *J. Mater. Chem.*, 2013, **1**, 500–504.
72 K. R. Paton, *et al.*, *Nat. Mater.*, 2014, **13**, 624–630.
73 S. Praneetha and A. Vadivel Murugan, *RSC Adv.*, 2013, **3**, 25403–25409.
74 B. Wang, D. Wang, Q. Wang, T. Liu, C. Guo and X. Zhao, *J. Mater. Chem. A*, 2013, **1**, 135–144.
75 J. Li, L. Zhang, L. Zhang, W. Hao, H. Wang, Q. Qu and H. Zheng, *J. Power Sources*, 2014, **249**, 311–319.
76 W. B. Luo, S. L. Chou, Y. C. Zhai and H. K. Liu, *J. Mater. Chem. A*, 2014, **2**, 4927–4931.
77 J. Ha, S. K. Park, S. H. Yu, A. Jin, B. Jang, S. Bong, I. Kim, Y. E. Sung and Y. Piao, *Nanoscale*, 2013, **5**, 8647–8655.
78 Y. Zhou, J. Wang, Y. Hu, R. O'Hayre and Z. Shao, *Chem. Commun.*, 2010, **46**, 7151–7153.
79 M. Chen, C. Du, B. Song, K. Xiong, G. Yin, P. Zuo and X. Cheng, *J. Power Sources*, 2013, **223**, 100–106.
80 J. P. Jegal and K. B. Kim, *J. Power Sources*, 2013, **243**, 859–864.
81 P. Manikandan, P. Periasamy and R. Jagannathan, *J. Mater. Chem. A*, 2013, **1**, 15397–15405.
82 G. Qin, Q. Wu, J. Zhao, Q. Ma and C. Wang, *J. Power Sources*, 2014, **248**, 588–595.
83 L. Dimesso, C. Spanheimer, W. Jaegermann, Y. Zhang and A. L. Yarin, *J. Appl. Phys.*, 2012, **111**, 064307.
84 L. Dimesso, C. Förster, W. Jaegermann, J. P. Khanderi, H. Tempel, A. Popp, J. Engstler, J. J. Schneider, A. Sarapulova, D. Mikhailova, L. A. Schmitt, S. Oswald and H. Ehrenberg, *Chem. Soc. Rev.*, 2012, **41**, 5068–5080.
85 C. Gong, Z. Xue, X. Wang, X. P. Zhou, X. L. Xie and Y. W. Mail, *J. Power Sources*, 2014, **246**, 260–268.
86 J. Yang, J. Wang, Y. Tang, D. Wang, B. Xiao, X. Li, R. Li, G. Liang, T. K. Sham and X. Sun, *J. Mater. Chem. A*, 2013, **1**, 7306–7311.
87 G. Wang, H. Liu, J. Liu, S. Qiao, G. M. Lu, P. Munroe and H. Ahn, *Adv. Mater.*, 2010, **22**, 4944–4948.
88 R. Wu, G. Xia, S. Shen, F. Zhu, F. Jiang and J. Zhang, *RSC Adv.*, 2014, **4**, 21325–21331.
89 T. Wumair, J. Dou, L. Zhang, M. Chen and X. Kang, *Ionics*, 2013, **19**, 1855–1860.
90 J. Zhu, J. Fiore, D. Li, N. M. Kinsinger, Q. Wang, E. DiMasi, J. Guo and D. Kisailus, *Cryst. Growth Des.*, 2013, **13**, 4659–4666.
91 Z. Ma, G. Shao, Y. Fan, G. Wang, J. Song and T. Liu, *ACS Appl. Mater. Interfaces*, 2014, **6**(12), 9236–9244.
92 X. Qin, J. Wang, J. Xie, F. Li, L. Wen and X. Wang, *Phys. Chem. Chem. Phys.*, 2012, **14**, 2669–2677.
93 K. M. Ø. Jensen, M. Christensen, H. P. Gunnlaugsson, N. Lock, E. D. Bøjesen, T. Proffen and B. B. Iversen, *Chem. Mater.*, 2013, **25**(11), 2282–2290.
94 M. Y. Cho, K. B. Kim, J. W. Lee, H. Kim, H. Kim, K. Kang and K. C. Roh, *RSC Adv.*, 2013, **3**, 3421–3427.
95 L. Wang, F. Zhou, Y. S. Meng and G. Ceder, *Phys. Rev. B: Condens. Matter Mater. Phys.*, 2007, **76**, 165435.

96 K. Saravanan, P. Balaya, M. V. Reddy, B. V. R. Chowdari and J. J. Vittal, *Energy Environ. Sci.*, 2010, **3**, 457–463.
97 R. Mei, X. Song, Y. Yang, Z. An and J. Zhang, *RSC Adv.*, 2014, **4**, 5746–5752.
98 K. A. Persson, B. Waldwick, P. Lazic and G. Ceder, *Phys. Rev. B: Condens. Matter Mater. Phys.*, 2012, **85**, 235438.
99 C. Nan, J. Lu, C. Chen, Q. Peng and Y. Li, *J. Mater. Chem.*, 2011, **21**, 9994–9996.
100 W. Kang, C. Zhao, R. Liui, F. Xu and Q. Shen, *CrystEngComm*, 2012, **14**, 2245–2250.
101 Y. Zhao, L. Peng, B. Liu and G. Yu, *Nano Lett.*, 2014, **14**(5), 2849–2853.
102 B. Guo, H. Ruan, C. Zheng, H. Fei and M. Wei, *Sci. Rep.*, 2013, **3**, 2788.
103 Y. Wang, Y. Wang, E. Hosono, K. Wang and H. Zhou, *Angew. Chem., Int. Ed.*, 2008, **47**, 7461–7465.
104 X. Zhang, Z. Bi, W. He, G. Yang, H. Liu and Y. Yue, *Energy Environ. Sci.*, 2014, **7**, 2285–2294.
105 J. Liu, M. N. Banis, Q. Sun, A. Lushington, R. Li, T. K. Sham and X. Sun, *Adv. Mater.*, 2014, **26**, 6472–6477.
106 J. Du, L. Jiao, Q. Wu, Y. Liu, Z. Qi, L. Guo, Y. Wang and H. Yuan, *Electrochim. Acta*, 2013, **98**, 288–293.
107 S. Ju, T. Liu, H. Peng, G. Li and K. Chen, *Mater. Lett.*, 2013, **93**, 194–198.
108 J. K. Kim, *CrystEngComm*, 2014, **16**, 2818–2822.
109 F. Yu, S. Lim, Y. Zhen, Y. An and J. Lin, *J. Power Sources*, 2014, **271**, 223–230.
110 Y. Jiang, S. Liao, Z. Liu, G. Xiao, Q. Liu and H. Song, *J. Mater. Chem. A*, 2013, **1**, 4546–4551.
111 M. Y. Cho, H. Kim, H. Kim, Y. S. Lim, K. B. Kim, J. W. Lee, K. Kang and K. C. Roh, *J. Mater. Chem. A*, 2014, **2**, 5922–5927.
112 W. K. Kim, W. H. Ryu, D. W. Han, S. J. Lim, J. Y. Eom and H. S. Kwon, *ACS Appl. Mater. Interfaces*, 2014, **6**(7), 4731–4736.
113 M. E. Schuster, D. Teschner, J. Popovic, N. Ohmer, F. Girgsdies, J. Tornow, M. G. Willinger, D. Samuelis, M. M. Titirici, J. Maier and R. Schlögl, *Chem. Mater.*, 2014, **26**(2), 1040–1047.
114 W. Sigle, R. Amin, K. Weichert, P. A. van Akena and J. Maier, *Electrochem. Solid-State Lett.*, 2009, **12**, A151–A154.
115 L. Laffont, C. Delacourt, P. Gibot, M. Y. Wu, P. Kooyman, C. Masquelier and J. Marie Tarascon, *Chem. Mater.*, 2006, **18**(23), 5520–5529.
116 S. Y. Chung, J. T. Bloking and Y. M. Chiang, *Nat. Mater.*, 2002, **1**, 123–128.
117 N. Ravet, A. Abouimrane and M. Armand, *Nat. Mater.*, 2003, **2**, 702.
118 P. S. Herle, B. Ellis, N. Coombs and L. F. Nazar, *Nat. Mater.*, 2004, **3**, 147–152.
119 M. Wagemaker, B. L. Ellis, D. Lutzenkirchen-hecht, F. M. Mulder and L. F. Nazar, *Chem. Mater.*, 2008, **20**, 6313–6315.
120 N. Meethong, Y. H. Kao, W. C. Carter and Y. M. Chiang, *Chem. Mater.*, 2010, **22**, 1088–1097.
121 N. Meethong, Y. H. Kao, S. A. Speakman and Y. M. Chiang, *Adv. Funct. Mater.*, 2009, **19**, 1060–1070.
122 M. S. Islam, D. J. Driscoll, C. A. J. Fisher and P. R. Slater, *Chem. Mater.*, 2005, **17**, 5085–5092.
123 Z. Ma, G. Shao, G. Wang, J. Du and Y. Zhang, *Ionics*, 2013, **19**, 437–443.
124 H. Fang, G. Liang, L. Zhao, T. Wallace, H. Arava, L. L. Zhang, A. Lgnatov and M. C. Croft, *J. Electrochem. Soc.*, 2013, **160**, A3148–A3152.
125 A. Moretti, G. Giuli, F. Nobili, A. Trapananti, G. Aquilanti, R. Tossici and R. Marassi, *J. Electrochem. Soc.*, 2013, **160**, A940–A949.
126 P. Zhang, Y. Wang, M. Lin, D. Zhang, X. Ren and Q. Yuan, *J. Electrochem. Soc.*, 2012, **159**, A402–A409.
127 J. Hong, X. L. Wang, Q. Wang, F. Omenya, N. A. Chernova, M. S. Whittingham and J. Graetz, *J. Phys. Chem. C*, 2012, **116**, 20787–20793.
128 L. L. Zhang, G. Liang, A. Ignatov, M. C. Croft, X. Q. Xiong, I. M. Hung, Y. H. Huang, X. L. Hu, W. X. Zhang and Y. L Peng, *J. Phys. Chem. C*, 2011, **115**, 13520–13527.
129 F. Omenya, N. A. Chernova, S. Upreti, P. Y. Zavalij, K. W. Nam, X. Q. Yang and M. S. Whittingham, *Chem. Mater.*, 2011, **23**, 4733–4740.
130 F. Omenya, N. A. Chernova, R. Zhang, J. Fang, Y. Huang, F. Cohen, N. Dobrzynski, S. Senanayake, W. Xu and M. S. Whittingham, *Chem. Mater.*, 2013, **25**, 85–89.
131 F. Omenya, N. A. Chernova, Q. Wang, R. Zhang and M. S. Whittingham, *Chem. Mater.*, 2013, **25**, 2691–2699.
132 K. L. Harrison, C. A. Bridges, M. P. Paranthaman, C. U. Segre, J. Katsoudas, V. A. Maroni, J. C. Idrobo, J. B. Goodenough and A. Manthiram, *Chem. Mater.*, 2013, **25**, 768–781.
133 C. Li, N. Hua, C. Wang, X. Kang, T. Wumair and Y. Han, *J. Alloys Compd.*, 2011, **509**, 1897–1900.
134 Q. Liu, Z. Liu, G. Xiao and S. Liao, *Ionics*, 2013, **19**, 445–450.
135 O. Čech, J. E. Thomas, A. Visintin, M. Sedlarikova, J. Vondráke and S. Moreno, *ECS Trans.*, 2012, **40**, 93–98.
136 B. Wang, B. Xu, T. Liu, P. Liu, C. Guo, S. Wang, Q. Wang, Z. Xiong, D. Wang and X. S. Zhao, *Nanoscale*, 2012, **6**, 986–995.
137 H. Zhang, Y. Tang, J. Shen, X. Xin, L. Cui, L. Chen, C. Ouyang, S. Shi and L. Chen, *Appl. Phys. A*, 2011, **104**, 529–537.
138 F. Omenya, B. Wen, J. Fang, R. Zhang, Q. Wang, N. A. Chernova, J. Schneider-Haefner, F. Cosandey and M. S. Whittingham, *Adv. Energy Mater.*, 2014, DOI: 10.1002/aenm.201401204.
139 J. Ni, Y. Zhao, J. Chen, L. Gao and L. Lu, *Electrochem. Commun.*, 2014, **44**, 4–7.
140 Z. H. Wang, L. X. Yuan, M. Wu, D. Sun and Y. H. Huang, *Electrochim. Acta*, 2011, **56**, 8477–8483.
141 F. Lu, Y. Zhou, J. Liu and Y. Pan, *Electrochim. Acta*, 2011, **56**, 8833–8838.
142 N. N. Bramnik, K. Nikolowski, C. Baehtz, K. G. Bramnik and H. Ehrenberg, *Chem. Mater.*, 2007, **19**(4), 908–915.
143 M. Okubo, D. Asakura, Y. Mizuno, J.-D. Kim, T. Mizokawa, T. Kudo and I. Honma, *J. Phys. Chem. Lett.*, 2010, **1**(14), 2063–2071.

144 A. Yamada, H. Koizumi, N. Sonoyama and R. Kanno, *Electrochem. Solid-State Lett.*, 2005, **8**(8), A409–A413.
145 C. Delmas, M. Maccario, L. Croguennec, F. Le Cras and F. Weill, *Nat. Mater.*, 2008, **7**, 665–671.
146 D. Burch and M. Z. Bazant, *Nano Lett.*, 2009, **9**(11), 3795–3800.
147 T. Sasaki, Y. Ukyo and P. Novak, *Nat. Mater.*, 2013, **12**, 569–575.
148 A. S. Andersson and J. O. Thomas, *J. Power Sources*, 2001, **97–98**, 498–502.
149 G. Chen, X. Song and T. J. Richardson, *J. Electrochem. Soc.*, 2007, **154**, A627–A632.
150 G. Kobayashi, S. Nishimura, M. S. Park, R. Kanno, M. Yashima, T. Ida and A. Yamada, *Adv. Funct. Mater.*, 2009, **19**, 395–403.
151 U. S. Kasavajjula, C. Wang and P. E. Arce, *J. Electrochem. Soc.*, 2008, **155**, A866–A874.
152 L. J. M. Davis, I. Heinmaa, B. L. Ellis, L. F. Nazar and G. R. Goward, *Phys. Chem. Chem. Phys.*, 2011, **13**, 5171–5177.
153 M. Farkhondeh, M. Safari, M. Pritzker, M. Fowler, T. Han, J. Wang and C. Delacourt, *J. Electrochem. Soc.*, 2014, **161**, A201–A212.
154 R. Malik, A. Abdellahi and G. Ceder, *J. Electrochem. Soc.*, 2013, **160**, A3179–A3197.
155 K. Weichert, W. Sigle, P. A. van Aken, J. Jamnik, C. Zhu, R. Amin, T. Acartürk, U. Starke and J. Maier, *J. Am. Chem. Soc.*, 2012, **134**(6), 2988–2992.
156 N. Meethong, H.-Y. S. Huang, S. A. Speakman, W. C. Carter and Y.-M. Chiang, *Adv. Funct. Mater.*, 2007, **17**, 1115–1123.
157 U. Boesenberg, *et al.*, *Chem. Mater.*, 2013, **25**(9), 1664–1672.
158 W. C. Chueh, F. E. Gabaly, J. D. Sugar, N. C. Bartelt, A. H. McDaniel, K. R. Fenton, K. R. Zavadil, T. Tyliszczak, W. Lai and K. F. McCarty, *Nano Lett.*, 2013, **13**(3), 866–872.
159 J. Wang, Y. K. Chen-Wiegart and J. Wang, *Nat. Commun.*, 2014, **5**, 4570.
160 G. Chen, X. Song and T. Richardson, *Electrochem. Solid-State Lett.*, 2006, **9**, A295–A298.
161 D. A. Cogswell and M. Z. Bazant, *ACS Nano*, 2012, **6**, 2215–2225.
162 N. Meethong, H. Y. S. Huang, W. C. Carter and Y. M. Chiang, *Electrochem. Solid-State Lett.*, 2007, **5**, A134–A138.
163 C. Delacourt, P. Poizot, J.-M. Tarascon and C. Masquelier, *Nat. Mater.*, 2005, **4**, 254–260.
164 F. Zhou, T. Maxisch and G. Ceder, *Phys. Rev. Lett.*, 2006, **97**, 155704.
165 X. J. Wang, H. Y. Chen, X. Yu, L. Wu, K. W. Nam, J. Bai, X. Huang and X. Q. Yang, *Chem. Commun.*, 2011, **47**, 7170–7172.
166 L. Gu, C. Zhu, H. Li, Y. Yu, C. Li, S. Tsukimoto, J. Maier and Y. Ikuhara, *J. Am. Chem. Soc.*, 2011, **133**(13), 4661–4663.
167 P. Gibot, M. Casas-Cabanas, L. Laffont, S. Levasseur, P. Carlach, S. Hamelet, J.-M. Tarascon and C. Masquelier, *Nat. Mater.*, 2008, **7**, 741–747.
168 Y. Zhu, J. W. Wang, Y. Liu, X. Liu, A. Kushima, Y. Liu, Y. Xu, S. X. Mao, J. Li, C. Wang and J. Y. Huang, *Adv. Mater.*, 2013, **11**, 5461–5466.
169 B. Ellis, L. K. Perry, D. H. Ryan and L. F. Nazar, *J. Am. Chem. Soc.*, 2006, **128**(35), 11416–11422.
170 L. Gu, C. Zhu, H. Li, Y. Yu, C. Li, S. Tsukimoto, J. Maier and Y. Ikuhara, *J. Am. Chem. Soc.*, 2011, **133**(13), 4661–4663.
171 L. Suo, W. Han, X. Lu, L. Gu, Y. S. Hu, H. Li, D. Chen, L. Chen, S. Tsukimoto and Y. Ikuhara, *Phys. Chem. Chem. Phys.*, 2012, **14**(16), 5363–5367.
172 C. Zhu, L. Gu, L. Suo, J. Popovic, H. Li, Y. Ikuhara and J. Maier, *Adv. Funct. Mater.*, 2014, **24**, 312–318.
173 X. Zhang, M. van Hulzen, D. P. Singh, A. Brownrigg, J. P. Wright, N. H. van Dijk and M. Wagemaker, *Nano Lett.*, 2014, **14**, 2279–2285.
174 Y. Sun, X. Lu, R. Xiao, H. Li and X. Huang, *Chem. Mater.*, 2012, **24**(24), 4693–4703.
175 J. Niu, A. Kushima, X. Qian, L. Qi, K. Xiang, Y. M. Chiang and J. Li, *Nano Lett.*, 2014, **14**(7), 4005–4010.
176 S. F. Amalraj and D. Aurbach, *J. Solid State Electrochem.*, 2011, **15**, 877–890.
177 X. Liu, W. Yang and Z. Liu, *Adv. Mater.*, 2014, **26**, 7710–7729.
178 J. McBreen, *J. Solid State Electrochem.*, 2009, **13**, 1051–1061.
179 Y. Orikasa, T. Maeda, Y. Koyama, H. Murayama, K. Fukuda, H. Tanida, H. Arai, E. Matsubara, Y. Uchimoto and Z. Ogumi, *J. Am. Chem. Soc.*, 2013, **135**(15), 5497–5500.
180 H. Liu, F. C. Strobridge, O. J. Borkiewicz, K. M. Wiaderek, K. W. Chapman, P. J. Chupas and C. P. Grey, *Science*, 2014, **344**, 1252817.
181 J. Zhou, J. Wang, L. Zuin, T. Regier, Y. Hu, H. Wang, Y. Liang, J. Maley, R. Sammynaiken and H. Dai, *Phys. Chem. Chem. Phys.*, 2012, **14**, 9578–9581.
182 T. Muraliganth and A. Manthiram, *J. Phys. Chem. C*, 2010, **114**(36), 15530–15540.
183 D. B. Ravnsbæk, K. Xiang, W. Xing, O. J. Borkiewicz, K. M. Wiaderek, P. Gionet, K. W. Chapman, P. J. Chupas and Y.-M. Chiang, *Nano Lett.*, 2014, **14**(3), 1484–1491.
184 F. Omenya, J. K. Miller, J. Fang, B. Wen, R. Zhang, Q. Wang, N. A. Chernova and M. S. Whittingham, *Chem. Mater.*, 2014, **26**, 6206–6212.
185 J. Kim, H. Kim, I. Park, Y. U. Park, J. K. Yoo, K. Y. Park, S. Lee and K. Kang, *Energy Environ Sci.*, 2013, **6**, 830–834.
186 Q. Liu, H. He, Z. F. Li, Y. Liu, Y. Ren, W. Lu, J. Lu, E. A. Stach and J. Xie, *ACS Appl. Mater. Interfaces*, 2014, **6**(5), 3282–3289.
187 N. Sharma, X. Guo, G. Du, Z. Guo, J. Wang, Z. Wang and V. K. Peterson, *J. Am. Chem. Soc.*, 2012, **134**(18), 786–7873.
188 W. Dreyer, J. Jamnik, C. Guhlke, R. Huth, J. Moškon and M. Gaberščček, *Nat. Mater.*, 2010, **9**, 448–453.
189 M. R. Roberts, A. Madsen, C. Nicklin, J. Rawle, M. G. Palmer, J. R. Owen and A. L. Hector, *J. Phys. Chem. C*, 2014, **118**(13), 6548–6557.
190 D. Robert, T. Douillard, A. Boulineau, G. Brunetti, P. Nowakowski, D. Venet, P. B. Guillemaud and C. Cayron, *ACS Nano*, 2013, **7**(12), 10887–10894.

191 X. Liu, D. Wang, G. Liu, V. Srinivasan, Z. Liu, Z. Hussain and W. Yang, *Nat. Commun.*, 2013, **4**, 2568.
192 D. A. Shapiro, *et al.*, *Nat. Photonics*, 2014, **8**, 765–769.
193 B. Kang and G. Ceder, *Nature*, 2009, **458**, 190–193.
194 G. Tan, F. Wu, L. Li, R. Chen and S. Chen, *J. Phys. Chem. C*, 2013, **117**, 6013–6021.
195 J. L. Allen, T. Richard Jow and J. Wolfenstine, *Chem. Mater.*, 2007, **19**(8), 2108–2111.
196 X. Wang, H. Yoshitake, Y. Masaki and H. Wang, *Electrochim. Acta*, 2014, **130**, 532–536.
197 J. Wang, J. Yang, Y. Tang, J. Liu, Y. Zhang, G. Liang, M. Gauthier, Y. K. Chen-Wiegart, M. N. Nanis, X. Li, R. Li, J. Wang, T. K. Sham and X. Sun, *Nat. Commun.*, 2014, **5**, 3415.
198 M. Koltypin, D. Aurbach, L. Nazar and B. Ellis, *Electrochem. Solid-State Lett.*, 2007, **10**, A40–A44.
199 W. Porcher, P. Moreau, B. Lestriez, S. Jouanneau and D. Guyomard, *Electrochem. Solid-State Lett.*, 2008, **11**, A4–A8.
200 M. Koltypin, D. Aurbach, L. Nazar and B. Ellis, *J. Power Sources*, 2007, **174**, 1241–1250.
201 K. Amine, J. Liu and I. Belharouak, *Electrochem. Commun.*, 2005, **7**, 669–673.
202 M. Safari and C. Delacourt, *J. Electrochem. Soc.*, 2011, **158**, A1436–A1447.
203 M. Dubarry, B. Y. Liaw, M. S. Chen, S. S. Chyan, K. C. Han, W. T. Sie and S. H. Wu, *J. Power Sources*, 2011, **196**, 3420–3425.
204 H. Song, Z. Cao, X. Chen, H. Lu, M. Jia, Z. Zhang, Y. Lai, J. Li and Y. Liu, *J. Solid State Electrochem.*, 2013, **17**, 599–605.
205 J. F. Martin, M. Cuisinier, N. Dupré, A. Yamada, R. Kanno and D. Guyomard, *J. Power Sources*, 2011, **196**, 2155–2163.
206 X. Chen, W. Xu, M. H. Engelhard, J. Zheng, Y. Zhang, F. Ding, J. Qian and J. G. Zhang, *J. Mater. Chem. A*, 2014, **2**, 2346–2352.
207 T. Waldmann, S. Gorse, T. Samtleben, G. Schneider, V. Knoblauch and M. Wohlfahrt-Mehrens, *J. Electrochem. Soc.*, 2014, **161**, A1742–A1747.
208 M. B. Pinson and M. Z. Bazant, *J. Electrochem. Soc.*, 2013, **160**, A243–A250.
209 M. Cuisinier, J. F. Martin, N. Dupré, A. Yamada, R. Kanno and D. Guyomard, *Electrochem. Commun.*, 2010, **12**, 238–241.
210 W. Porcher, P. Moreau, B. Lestriez, S. Jouanneau, F. Le Cras and D. Guyomard, *Ionics*, 2008, **14**, 583–587.
211 J. Wang, J. Yang, Y. Tang, R. Li, G. Liang, T. K. Sham and X. Sun, *J. Mater. Chem. A*, 2013, **1**, 1579–1586.
212 K. Zaghib, A. Mauger, F. Gendron and C. M. Julien, *Chem. Mater.*, 2008, **20**(2), 462–469.
213 M. Gauthier, C. Michot, N. Ravet, M. Duchesneaua, J. Dufour, G. Liang, J. Wontcheu, L. Gauthier and D. D. MacNeil, *J. Electrochem. Soc.*, 2010, **157**, A453–A462.
214 G. Kear, B. D. Barker and F. C. Walsh, *Corros. Sci.*, 2004, **46**, 109–135.
215 J. Wang, Y. Tang, J. Yang, R. Li, G. Liang and X. Sun, *J. Power Sources*, 2013, **238**, 454–463.
216 S. A. Channagiri, S. C. Nagpure, S. S. Babua, G. J. Noble and R. T. Hart, *J. Power Sources*, 2013, **243**, 750–757.
217 M. D. Slater, D. Kim, E. Lee and C. S. Johnson, *Adv. Funct. Mater.*, 2013, **23**, 947–958.
218 V. Palomares, P. Serras, I. Villaluenga, K. B. Hueso, J. Carretero-González and T. Rojo, *Energy Environ. Sci.*, 2012, **5**, 5884–5901.
219 S. W. Kim, D. H. Seo, X. Ma, G. Ceder and K. Kang, *Adv. Energy Mater.*, 2012, **2**, 710–721.
220 K. Zaghib, J. Trottier, P. Hovington, F. Brochu, A. Guerfi, A. Mauger and C. M. Julien, *J. Power Sources*, 2011, **196**, 9612–9617.
221 S. M. Oh, S. T. Myung, J. Hassound, B. Scrosati and Y. K. Sun, *Electrochem. Commun.*, 2012, **22**, 149–152.
222 K. T. Lee, T. N. Ramesh, F. Nan, G. Botton and L. F. Nazar, *Chem. Mater.*, 2011, **23**(16), 3593–3600.
223 J. Gaubicher, F. Boucher, P. Moreau, M. Cuisinier, P. Soudan, E. Elkaim and D. Guyomard, *Electrochem. Commun.*, 2014, **38**, 104–106.
224 P. Moreau, D. Guyomard, J. Gaubicher and F. Boucher, *Chem. Mater.*, 2010, **22**(14), 4126–4128.
225 M. Casas-Cabanas, V. V. Roddatis, D. Saurel, P. Kubiak, J. Carretero-Gonzales, V. Palomares, P. Serras and T. Rojo, *J. Mater. Chem.*, 2012, **22**, 17421–17423.
226 J. Lu, S. C. Chung, S. Nishimura and A. Yamada, *Chem. Mater.*, 2013, **25**(22), 4557–4565.
227 M. Galceran, D. Saurel, B. Acebedo, V. V. Roddatis, E. Martin, T. Rojo and M. Casas-Cabanas, *Phys. Chem. Chem. Phys.*, 2014, **16**, 8837–8842.
228 M. Galceran, V. Roddatis, F. J. Zuniga, J. M. Perez-Mato, B. Acebedo, R. Arenal, I. Peral, T. Rojo and M. Casas-Cabanas, *Chem. Mater.*, 2014, **26**, 3289–3294.
229 J. Sugiyama, H. Nozaki, M. Harada, Y. Higuchi, J. H. Brewer, E. J. Ansaldo, G. Kobayashi and R. Kanno, *Phys. Rev. B: Condens. Matter Mater. Phys.*, 2014, **90**, 014426.
230 F. Boucher, J. Gaubicher, M. Cuisinier, D. Guyomard and P. Moreau, *J. Am. Chem. Soc.*, 2014, **136**(25), 9144–9157.
231 R. Tripathi, S. M. Wood, M. S. Islam and L. F. Nazar, *Energy Environ. Sci.*, 2013, **6**, 2257–2264.
232 Y. Zhu, Y. Xu, Y. Liu, X. Luo and C. Wang, *Nanoscale*, 2013, **5**, 780–787.
233 M. Avdeev, Z. Mohamed, C. D. Ling, J. Lu, M. Tamaru, A. Yamada and P. Barpanda, *Inorg. Chem.*, 2013, **52**, 8685–8693.
234 P. P. Prosini, C. Cento, A. Masci and M. Carewska, *Solid State Ionics*, 2014, **263**, 1–8.
235 H. Pan, Y. S. Hu and L. Chen, *Energy Environ. Sci.*, 2013, **6**, 2338–2360.
236 S. Y. Hong, Y. Kim, Y. Park, A. Choi, N. S. Choi and K. T. Lee, *Energy Environ. Sci.*, 2013, **6**, 2067–2081.
237 V. Palomares, M. Casas-Cabanas, E. Castillo-Martínez, M. H. Han and T. Rojo, *Energy Environ. Sci.*, 2013, **6**, 2312–2337.
238 J. Trottier, P. Hovington, F. Brochu, I. Rodrigues, K. Zaghib, A. Mauger and C. M. Julien, *ECS Trans.*, 2011, **35**, 123–128.
239 I. Hasa, J. Hassoun, Y. K. Sun and B. Scrosati, *ChemPhysChem*, 2014, **15**, 2152–2155.
240 P. Moreau, D. Guyomard, J. Gaubicher and F. Boucher, *Chem. Mater.*, 2010, **22**(14), 4126–4128.

241 Y. Yin, Y. Hu, P. Wu, H. Zhang and C. Cai, *Chem. Commun.*, 2012, **48**, 2137–2139.
242 J. Zhao, Z. Jian, J. Ma, F. Wang, Y. S. Hu, W. Chen, L. Chen, H. Liu and S. Dai, *ChemSusChem*, 2012, **5**, 1495–1500.
243 Y. Liu, Y. Xu, X. Han, C. Pellegrinelli, Y. Zhu, H. Zhu, J. Wan, A. C. Chung, O. Vaaland, C. Wang and L. Hu, *Nano Lett.*, 2012, **12**(11), 5664–5668.
244 Y. S. Hong, K. S. Ryu, Y. J. Park, M. G. Kim, J. M. Lee and S. H. Chang, *J. Mater. Chem.*, 2002, **12**, 1870–1874.
245 S. Xu, S. Zhang, J. Zhang, T. Tan and Y. Liu, *J. Mater. Chem. A*, 2014, **2**, 7221–7228.
246 J. P. Jegal, J. G. Kim and K. B. Kim, *Electrochem. Commun.*, 2013, **30**, 87–90.
247 Q. Fan, L. Lei, G. Yin, Y. Chen and Y. Sun, *Electrochem. Commun.*, 2014, **38**, 120–123.
248 Y. Fang, L. Xiao, J. Qian, X. Ai, H. Yang and Y. Cao, *Nano Lett.*, 2014, **14**(6), 3539–3543.
249 B. L. Ellis, W. R. M. Makahnouk, Y. Makimura, K. Toghill and L. F. Nazar, *Nat. Mater.*, 2007, **6**, 749–753.
250 W. Song, X. Ji, Z. Wu, Y. Zhu, Y. Yao, K. Huangfu, Q. Chen and C. E. Banks, *J. Mater. Chem. A*, 2014, **2**, 2571–2577.
251 N. V. Kosova, V. R. Podugolnikov, E. T. Devyatkina and A. B. Slobodyuk, *Mater. Res. Bull.*, 2014, **60**, 849–857.
252 Y. Kawabe, N. Yabuuchi, M. Kajiyama, N. Fukuhara, T. Inamasu, R. Okuyama, I. Nakai and S. Komana, *Electrochem. Commun.*, 2011, **13**, 1225–1228.
253 A. Langrock, Y. Xu, Y. Liu, S. Ehraman, A. Manivannan and C. Wang, *J. Power Sources*, 2013, **223**, 62–67.
254 D. D. MacNeil, L. Devigne, C. Michot, I. Rodrigues, G. Liang and M. Gauthier, *J. Electrochem. Soc.*, 2010, **157**(4), A463–A468.
255 S. M. Oh and Y. K. Sun, *J. Power Sources*, 2013, **244**, 663–667.
256 K. Zaghib, M. Trudeau, A. Guerfi, J. Trottier, A. Mauger, R. Veillette and C. M. Julien, *J. Power Sources*, 2012, **204**, 177–181.
257 Y. K. Sun, S. T. Myung, B. C. Park, J. Prakash, I. Belharouak and K. Amine, *Nat. Mater.*, 2009, **8**, 320–324.
258 Z. Q. Huo, Y. T. Cui, D. Wang, D. Yue and C. Li, *J. Power Sources*, 2014, **245**, 331–336.